

POISON-SPLAT: COMPUTATION COST ATTACK ON 3D GAUSSIAN SPLATTING

Anonymous authors

Paper under double-blind review

ABSTRACT

3D Gaussian splatting (3DGS), known for its groundbreaking performance and efficiency, has become a dominant 3D representation and brought progress to many 3D vision tasks. However, in this work, we reveal a significant security vulnerability that has been largely overlooked in 3DGS: **the computation cost of training 3DGS could be maliciously tampered by poisoning the input data**. By developing an attack named *Poison-splat*, we reveal a novel attack surface where the adversary can poison the input images to **drastically increase the computation memory and time** needed for 3DGS training, pushing the algorithm towards its worst computation complexity. In extreme cases, the attack can even consume all allocable memory, leading to a Denial-of-Service (DoS) that disrupts servers, resulting in practical damages to real-world 3DGS service vendors. Such a computation cost attack is achieved by addressing a bi-level optimization problem through three tailored strategies: attack objective approximation, proxy model rendering, and optional constrained optimization. These strategies not only ensure the effectiveness of our attack but also make it difficult to defend with simple defensive measures. We hope the revelation of this novel attack surface can spark attention to this crucial yet overlooked vulnerability of 3DGS systems.

1 INTRODUCTION

3D reconstruction, aiming to build 3D representations from multi-view 2D images, holds a critical position in computer vision and machine learning, extending its benefits across broad domains including entertainment, healthcare, archaeology, and the manufacturing industry. A notable example is Google Map with a novel feature for NeRF-based (Mildenhall et al., 2021) 3D outdoor scene reconstruction (Google, 2023). Similarly, commercial companies like LumaAI, KIRI, Polycam and Spline offer paid service for users to generate 3D captures from user-uploaded images or videos. Among these popular 3D applications, many are powered by a novel and sought-after 3D reconstruction paradigm known as 3D Gaussian Splatting (3DGS).

3DGS, introduced by Kerbl et al. (2023) in 2023, has quickly revolutionized the field of 3D Vision and achieved overwhelming popularity (Chen & Wang, 2024; Fei et al., 2024; Wu et al., 2024b; Dalal et al., 2024). 3DGS is not powered by neural networks, distinguishing itself from NeRF (Mildenhall et al., 2021), the former dominant force in 3D vision. Instead, it captures 3D scenes by learning a cloud of 3D Gaussians as an explicit 3D model and uses rasterization to render multiple objects simultaneously. This enables 3DGS to achieve significant advantages in rendering speed, photo-realism, and interpretability, making it a game changer in the field.

One intriguing property of Gaussian Splatting is its **flexibility in model complexity**. Unlike NeRF or any other neural-network based algorithms which have a pre-determined and fixed computational complexity based on network hyper-parameters, 3DGS can dynamically adjust its complexity according to the input data. During the 3DGS training process, the size of learnable parameters, *i.e.* the number of 3D Gaussians is dynamically adjusted to align with the complexity of the underlying 3D scene. More specifically, 3DGS algorithm uses an *adaptive density control* strategy to flexibly increase or decrease the number of Gaussians for optimizing reconstruction, leading to variable computational complexity in terms of GPU memory occupancy and training time cost.

The above flexibility in design aims to provide training advantages. However, this flexibility can also become a vulnerability. In this paper, we reveal a severe yet unnoticed attack vector: the flexibility of 3DGS complexity can be abused to over-consume computation resources such as GPU memory and

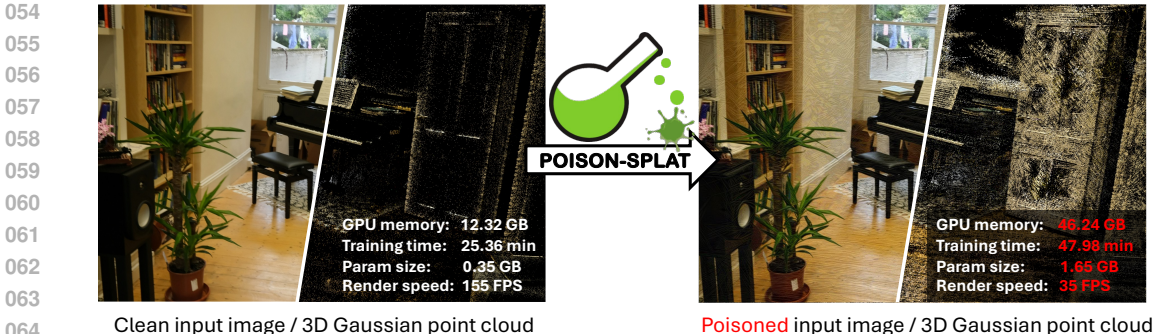


Figure 1: Our *Poison-splat* attack adds perturbations to input images, making 3D Gaussian Splatting need significantly more parameters to reconstruct the 3D scene, leading to huge increases in GPU memory consumption, training time and rendering latency. Here, we visualize the input image and the underlying 3D Gaussians of a clean view (left) and its corresponding poisoned view (right).

significantly drag down training speed of Gaussian Splatting system, pushing the training process to its worst computational complexity.

We develop a computation cost attack method named *Poison-splat* as a proof-of-concept of this novel attack vector. *Poison-splat* takes the form of training data poisoning (Tian et al., 2022), where the attacker manipulates the input data fed into the victim 3DGS system. This is practical in real-world scenarios, as commercial 3D service providers like Kiri (KIRI), Polycam (Polycam) and Spline (Spline) receive images or videos from end users to generate 3D captures. An attacker can hide themselves among normal users to submit poisoned data and launch the attack stealthily, or even secretly manipulate data uploaded by other users. During peak usage periods, this attack competes for computing resources with legitimate users, slowing down service response times and potentially causing severe consequences like service crashes, leading to significant financial losses for service providers.

We formulate *Poison-splat* attack as a max-min problem. The inner optimization is the learning process of 3D Gaussian Splatting, i.e., minimizing the reconstruction loss given a set of input images and camera poses, while the outer optimization problem is to maximize the computation cost of solving the inner problem. Although accurately solving this bi-level optimization is often infeasible, we find that the attacker can use a *proxy model* to approximate the inner minimization and focus on optimizing the outer maximization objective. Moreover, we observe an important relationship that memory consumption and rendering latency exhibit a clear positive correlation with the number of 3D Gaussians in training. Therefore, the attacker can use the number of Gaussians in proxy model training as a metric to depict computation costs for outer optimization. Motivated by these insights, our *Poison-splat* attack uses image total variation loss as a prior to guide the over-densification of 3D Gaussians, and can approximately solve this bi-level optimization problem in a cheap way.

The contributions of this work can be concluded in three-folds:

- We reveal that the flexibility in model complexity of 3DGS can become a security backdoor, making it vulnerable to computation cost attack. This vulnerability has been largely overlooked by the 3D vision and machine learning communities. Our research shows that such attacks are feasible, potentially causing severe financial losses to 3D service providers.
- We formulate the attack on 3D Gaussian Splatting as a data poisoning attack problem. To our best knowledge, there is no previous work investigating how to poison training data to increase the computation cost of machine learning systems.
- We propose a novel attack algorithm, named *Poison-splat*, which significantly increases GPU memory consumption and slows down training procedure of 3DGS. We hope the community can recognize this vulnerability and develop more robust 3D Gaussian Splatting algorithms or defensive methods to mitigate such attacks.

2 PRELIMINARIES

In this section, we provide essential backgrounds on 3D Gaussian Splatting and resource-targeting attacks, which are crucial for understanding our attack method proposed in Section 3. Due to page constraints, we put related works in Appendix Section A.

2.1 3D GAUSSIAN SPLATTING

3D Gaussian Splatting (3DGS) (Kerbl et al., 2023) has revolutionized the 3D vision community with its superior performance and efficiency. It models a 3D scene by learning a set of 3D Gaussians $\mathcal{G} = \{G_i\}$ from multi-view images $\mathcal{D} = \{V_k, P_k\}_{k=1}^N$, where each view consists of a ground-truth image V_k and the corresponding camera poses P_k . We denote N as the total number of image-pose pairs in the training data. As for the model, each 3D Gaussian $G_i = \{\mu_i, s_i, \alpha_i, q_i, c_i\}$ has 5 optimizable parameters: center coordinates μ_i , scales s_i , opacity α_i , rotation quaternion q_i , and associated view-dependent color represented as spherical harmonics c_i .

To render \mathcal{G} from 3D Gaussian space to 2D images, each Gaussian is first projected into the camera coordinate frame given a camera pose P_k to determine the depth of each Gaussian, which is the distance of that Gaussian to the camera view. The calculated depth is used for sorting Gaussians from near to far, and then the colors in 2D image are rendered in parallel by alpha blending according to the depth order of adjacent 3D Gaussians. We denote the 3DGS renderer as a function \mathcal{R} , which takes as input the Gaussians \mathcal{G} and a camera pose P_k to render an image $V'_k = \mathcal{R}(\mathcal{G}, P_k)$.

The training is done by optimizing the reconstruction loss between the rendered image and ground truth image for each camera view, where the reconstruction loss is a combination of \mathcal{L}_1 loss and structural similarity index measure (SSIM) loss $\mathcal{L}_{\text{D-SSIM}}$ (Brunet et al., 2011):

$$\min_{\mathcal{G}} \mathcal{L}(\mathcal{D}) = \min_{\mathcal{G}} \sum_{k=1}^N \mathcal{L}(V'_k, V_k) = \min_{\mathcal{G}} \sum_{k=1}^N (1 - \lambda) \mathcal{L}_1(V'_k, V_k) + \lambda \mathcal{L}_{\text{D-SSIM}}(V'_k, V_k), \quad (1)$$

where λ is a trade-off parameter. To ensure finer reconstruction, 3DGS deploys *adaptive density control* to automatically add or remove Gaussians from optimization. Adding Gaussians is called densification, while removing Gaussians is called pruning. Densification is performed when the view-space positional gradient $\nabla_{\mu_i} \mathcal{L}$ is larger than a pre-set gradient threshold τ_g (by default 0.0002). Pruning occurs when the opacity α_i falls below the opacity threshold τ_α . Both densification and pruning are non-differentiable operations. A more formal and comprehensive introduction is provided in Appendix Section B.

2.2 RESOURCE-TARGETING ATTACK

A similar concept in computer security domain is the Denial-of-Service (DoS) attack (Elleithy et al., 2005; Aldhyani & Alkahtani, 2023; Bhatia et al., 2018). A DoS attack aims to overwhelmly consume a system’s resources or network (Mirkovic & Reiher, 2004; Long & Thomas, 2001), making it unable to serve legitimate users. Common methods include flooding the system with excessive requests or triggering a crash through malicious inputs. Such attacks pose severe risks to real-world service providers, potentially resulting in extensive operational disruptions and financial losses. For example, Midjourney, a generative AI platform, experienced a significant 24-hour system outage (Akash, 2024), potentially caused by employees from another generative AI company who were allegedly scraping data, causing a Denial-of-Service.

In the machine learning community, similar concepts are rarely mentioned. This might stem from the fact that once hyper-parameters are set in most machine learning models, such as deep neural networks, their computation complexity remains fixed. Regardless of input data content, most machine learning algorithms incur nearly constant computational costs and consume almost consistent computational resources. Despite this, only a few studies have focused on **resource-targeting attacks at inference stage** of machine learning systems. For example, Shumailov et al. (2021) first identified samples that trigger excessive neuron activations which maximise energy consumption and latency. Following works investigated other inference-stage attacks against dynamic neural networks (Hong et al., 2020; Chen et al., 2023) and language models (Chen et al., 2022b;a; Gao et al., 2023). However, to our knowledge, no previous works have targeted at attacking the training-stage computation cost of machine learning systems. Our work is pioneering in bridging this research gap through Gaussian Splatting, which features adaptively flexible computation complexity.

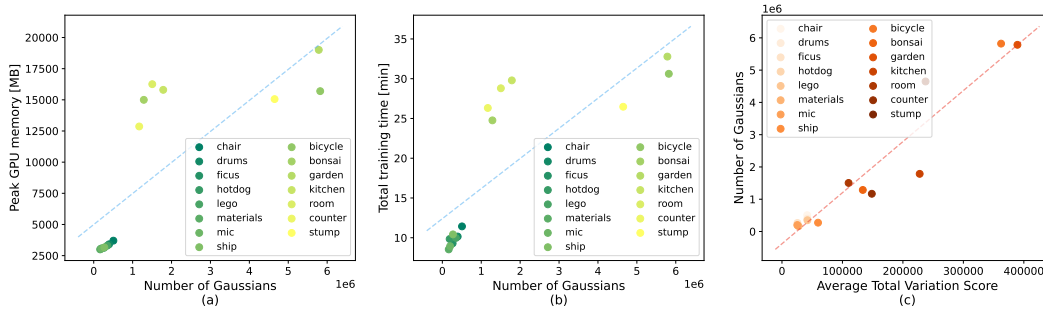


Figure 2: The figure illustrates the strong positive correlation between the number of Gaussians and (a) GPU memory occupancy, and (b) training time costs. Panel (c) shows the relationship between image sharpness, measured by the average total variation score, and the number of Gaussians.

3 POISON-SPLAT ATTACK

In this section, we first formulate the computation cost attack on 3D Gaussian Splatting in Section 3.1. Subsequently, we introduce a novel attack method in Section 3.2.

3.1 PROBLEM FORMULATION

We formulate our attack under data poisoning framework as follows. The victims are the service providers of 3D Gaussian Splatting (3DGS), who typically train their 3DGS models using a dataset of multi-view images and camera poses $\mathcal{D} = \{V_k, P_k\}_{k=1}^N$. We assume the attackers have the capability to introduce poisoned data within the entire dataset. This assumption is realistic as an attacker could masquerade as a regular user, submitting poisoned data covertly, or even covertly alter data submitted by legitimate users. This allows the attack to be launched stealthily and enhances its potential impact on the training process of 3DGS. We next detail the formulation of the attacker and victim.

Attacker. The attacker begins with the clean data $\mathcal{D} = \{V_k, P_k\}_{k=1}^N$ as input, manipulating it to produce poisoned training data $\mathcal{D}_p = \{\tilde{V}_k, P_k\}_{k=1}^N$, where the attacker does not modify the camera pose configuration files. Each poisoned image \tilde{V}_k is perturbed from the original clean image V_k , aiming to maximize the computational costs of victim training, such as GPU memory usage and training time. The ultimate goal of the attacker is to significantly increase the computational resources, potentially leading to a denial-of-service attack by overwhelming the training system.

Victim. On the other hand, the victim receives this poisoned dataset $\mathcal{D}_p = \{\tilde{V}_k, P_k\}_{k=1}^N$ from the attacker, unaware that it has been poisoned. With this data, the victim seeks to train a Gaussian Splatting Model \mathcal{G} , striving to minimize the reconstruction loss (cf. Eq. (1)). The victim’s objective is to achieve the lowest loss as possible, thus ensuring the quality of the Gaussian Splatting model.

Optimization problem. To summarize, the computation cost attack for the attacker can be formulated as the following max-min bi-level optimization problem:

$$\mathcal{D}_p = \arg \max_{\mathcal{D}_p} \mathcal{C}(\mathcal{G}^*), \quad \text{s.t.} \quad \mathcal{G}^* = \arg \min_{\mathcal{G}} \mathcal{L}(\mathcal{D}_p), \quad (2)$$

where the computation cost metric $\mathcal{C}(\mathcal{G})$ is flexible and can be designed by the attacker.

3.2 PROPOSED METHOD

To conduct the attack, directly addressing the above optimization is infeasible as the computation cost is not differentiable. To address this, we seek to find an approximation for the objective.

Using the number of Gaussians as an approximation. As is mentioned in Section 1, a major advantage of 3DGS is its flexibility to dynamically adjust model complexity (*i.e.*, the number of Gaussians) according to the complexity of the input data. This adaptability enhances the model’s efficiency and fidelity in rendering complex scenes. However, this feature may also act as a double-edged sword, providing a potential backdoor for attacks. To explore this, we analyze how the number of Gaussians affects computational costs, including memory consumption and training time. Our findings, depicted in Figures 2(a-b), reveal a clear positive correlation between computational costs

Algorithm 1 Poison-splat

Input: Clean dataset: $\mathcal{D} = \{V_k, P_k\}$; Perturbation range: ϵ ; Perturbation step size: η ;
The iteration number of inner optimization: T ; The iteration number of outer optimization: \tilde{T} .

Output: Poisoned dataset: $\mathcal{D}_p = \{\tilde{V}_k, P_k\}$

- 1: Initialize poisoned dataset: $\mathcal{D}_p = \mathcal{D}$
- 2: Train a Gaussian Splatting proxy model \mathcal{G}_p on clean dataset \mathcal{D} ▷ Eq. (1)
- 3: **For** $t = 1, \dots, T$ **do**
- 4: Sample a random camera view k
- 5: $V'_k = \mathcal{R}(\mathcal{G}_p, P_k)$ ▷ Get the rendered image under the camera view k
- 6: $\tilde{V}_k = V'_k$ ▷ Optimization of target image starts from rendered image
- 7: **For** $\tilde{t} = 1, \dots, \tilde{T}$ **do**
- 8: $\tilde{V}_k = \tilde{V}_k + \eta \cdot \text{sign}(\nabla_{\tilde{V}_k} \mathcal{S}_{TV}(\tilde{V}_k))$ ▷ Eq. (4)
- 9: $\tilde{V}_k = \mathcal{P}_\epsilon(\tilde{V}_k, V_k)$ ▷ Project into ϵ -ball, *i.e.*, Eq. (5)
- 10: **end While**
- 11: Update proxy model \mathcal{G}_p by minimizing $\mathcal{L}(V'_k, \tilde{V}_k)$ under current view ▷ Eq. (1)
- 12: Update poisoned dataset: $\mathcal{D}_p^k := (\tilde{V}_k, P_k)$ ▷ Update the k -th element of \mathcal{D}_p
- 13: **end While**

and the number of Gaussians used in rendering. In light of this insight, it is intuitive to use the number of Gaussians $\|\mathcal{G}\|$ to approximate the computation cost function involved in the inner optimization:

$$\mathcal{C}(\mathcal{G}) := \|\mathcal{G}\|. \quad (3)$$

Maximizing the number of Gaussians by sharpening 3D objects. Even with the above approximation, solving the optimization problem is still hard since the Gaussian densification operation in 3DGS is not differentiable. Hence, it would be infeasible for the attacker to use gradient-based methods to optimize the number of Gaussians. To circumvent this, we explore a strategic alternative. As shown in Figure 2(c), we find that 3DGS tends to assign more Gaussians to those objects with more complex structures and non-smooth textures, as quantified by the total variation score—a metric assessing image sharpness (Rudin et al., 1992). Intuitively, the less smooth the surface of 3D objects is, the more Gaussians the model needs to recover all the details from its 2D image projections. Hence, non-smoothness can be a good descriptor of complexity of Gaussians, *i.e.*, $\|\mathcal{G}\| \propto \mathcal{S}_{TV}(\mathcal{D})$. Inspired by this, we propose to maximize the computation cost by optimizing the total variation score of rendered images $\mathcal{S}_{TV}(\tilde{V}_k)$:

$$\mathcal{C}(\mathcal{G}) := \mathcal{S}_{TV}(\tilde{V}_k) = \sum_{i,j} \sqrt{|\tilde{V}_k^{i+1,j} - \tilde{V}_k^{i,j}|^2 + |\tilde{V}_k^{i,j+1} - \tilde{V}_k^{i,j}|^2}. \quad (4)$$

Balancing attack strength and stealthiness via optional constrained optimization. The above strategies enable the attack to significantly increase computational costs. However, this may induce an unlimited alteration to the image and result in a loss of semantic integrity in the generated view images (cf. Figure 4(b)), making it obvious to detect. Considering the strategic objectives of an adversary who may wish to preserve image semantics and launch the attack by stealth, we introduce an optional constrained optimization strategy. Inspired by adversarial attacks (Szegedy et al., 2013; Madry et al., 2018), we enforce a ϵ -ball constraint of the L_∞ norm on the perturbations:

$$\tilde{V}_k \in \mathcal{P}_\epsilon(\tilde{V}_k, V_k). \quad (5)$$

where $\mathcal{P}_\epsilon(\cdot)$ means to clamp the rendered poisoned image to be within the ϵ -ball of the L_∞ norm around the original clean image, *i.e.*, $\|\tilde{V}_k - V_k\|_\infty \leq \epsilon$. This constraint limits each pixel’s perturbation to a maximum of ϵ . By tuning ϵ , an attacker can balance the destructiveness and the stealthiness of the attack, allowing for strategic adjustments for the desired outcome. If ϵ is set to ∞ , the constraint is effectively removed, returning the optimization to its original, unconstrained form.

Ensuring multi-view image consistency via proxy model. An interesting insight from our study is that simply optimizing perturbations for each view image independently by maximizing total variation score does not effectively bolster attacks. As demonstrated in Figure 3(b), this image-level

TV-maximization attack is significantly less effective compared to our *Poison-splat* strategy. This mainly stems from the image-level optimization creating inconsistencies across the different views of poisoned images, undermining the attack’s overall effectiveness.

Our solution is inspired by the view-consistent properties of the 3DGS model’s rendering function, which effectively maintains consistency across multi-view images generated from 3D Gaussian space. In light of this, we propose to train a proxy 3DGS model to generate poisoned data. In each iteration, the attacker projects the current proxy model onto a camera pose, obtaining a rendered image V'_k . This image then serves as a starting point for optimization, where the attacker searches for a target \tilde{V}_k that maximizes the total variation score within the ϵ -bound of the clean image V_k . Following this, the attacker updates the proxy model with a single optimization step to mimic the victim’s behavior. In subsequent iterations, the generation of poisoned images initiates with the rendering output from the updated proxy model. In this way, the attacker approximately solves this bi-level optimization by iteratively unrolling the outer and inner optimization, enhancing the attack’s effectiveness while maintaining consistency across views. We summarize the pipeline of *Poison-splat* in Algorithm 1.

4 EXPERIMENTS

Datasets. All experiments in this paper are carried out on three common 3D datasets: (1) NeRF-Synthetic¹ (Mildenhall et al., 2021) is a synthetic 3D object dataset, which contains multi-view renderings of synthetic 3D objects. (2) Mip-NeRF360² dataset (Barron et al., 2022) is a 3D scene dataset, which is composed of photographs of large real-world outdoor scenes. (3) Tanks-and-Temples³ dataset (Knapitsch et al., 2017) contains realistic 3D captures including both outdoor scenes and indoor environments.

Implementation details. In our experiments, we use the official implementation of 3D Gaussian Splatting⁴ (Kerbl et al., 2023) to implement the victim behavior. Following their original implementation, we use the recommended default hyper-parameters, which were proved effective across a broad spectrum of scenes from various datasets. For testing black-box attack effectiveness, we use the official implementation of Scaffold-GS⁵ (Lu et al., 2024) as a black box victim. All experiments reported in the paper were carried out on a single NVIDIA A800-SXM4-80G GPU.

Evaluation metrics. We use the number of 3D Gaussians, GPU memory occupancy and the training time cost as metrics to evaluate the computational cost of 3DGS. A more successful attack is characterized by larger increases in the number of Gaussians, higher GPU memory consumption, and extended training time, compared with training on clean data. We also report the rendering speed of the resulted 3DGS models to show the increase in model complexity and degradation of inference latency as a byproduct of our attack.

4.1 MAIN RESULTS

We report the comparisons of the number of Gaussians, peak GPU memory, training time and rendering speed between clean and poisoned data across three different datasets in Tables 1 to show the effectiveness of our attack. The full results containing all scenes are listed in the Appendix Table 3 and Table 4. We provide visualizations of example poisoned datasets and corresponding victim reconstructions in Appendix Section F.

We want to highlight some observations from the results. First, our *Poison-splat* attack demonstrates the ability to craft a huge extra computational burden across multiple datasets. Even with perturbations constrained within a small range in an ϵ -constrained attack, the peak GPU memory can be increased to over 2 times, making the overall maximum GPU occupancy higher than 24 GB - in the real world, this may mean that our attack may require more allocable resources than common GPU stations can provide, e.g., RTX 3090, RTX 4090 and A5000. Furthermore, as we visualized the computational cost in Figure 3(a), the attack not only significantly increases the memory usage, but also greatly slows

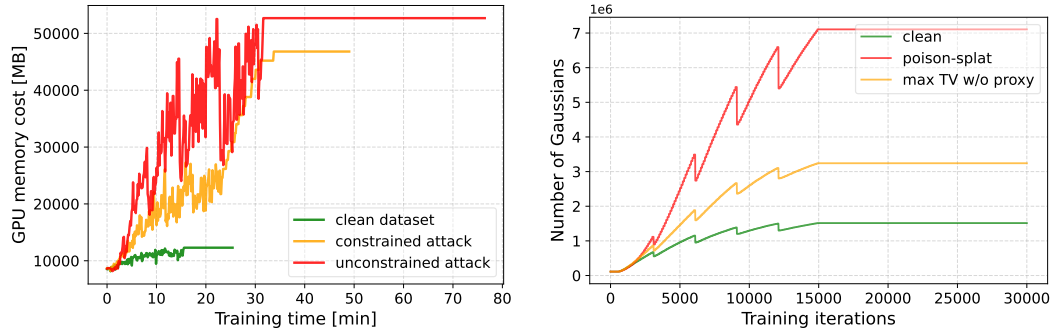
¹Dataset publicly accessible at <https://github.com/bmild/nerf>.

²Dataset publicly accessible at <https://jonbarron.info/mipnerf360/>

³Dataset publicly accessible at <https://www.tanksandtemples.org/download/>

⁴<https://github.com/graphdeco-inria/gaussian-splatting>

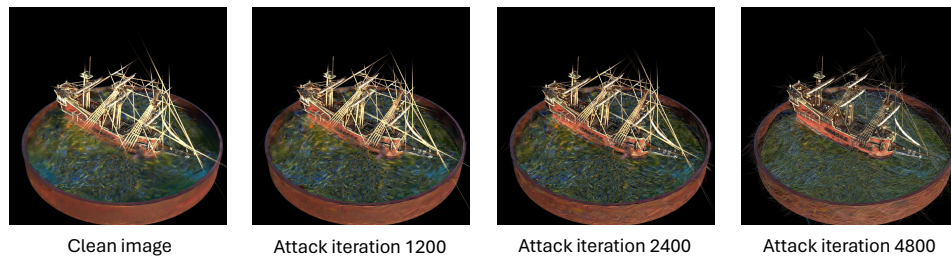
⁵<https://github.com/city-super/Scaffold-GS>



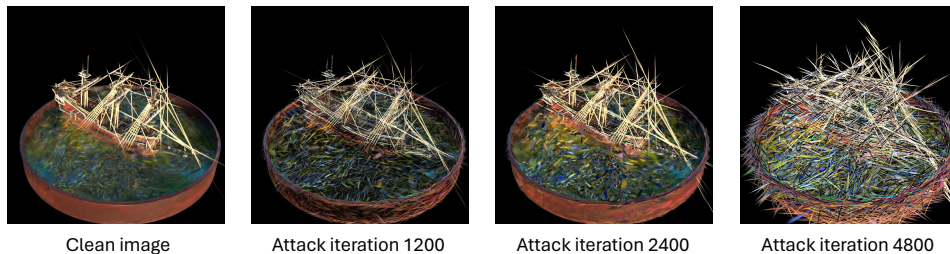
(a) Overall comparisons of computation cost in training time and GPU memory occupancy on MIP-NeRF360 (room). (b) Number of Gaussians needed for reconstruction under our attack, naive TV-maximization attack and on the clean data of MIP-NeRF360 (room).

Figure 3: Figure (a) shows that our attack leads to a significant increase on the GPU memory and training time. Figure (b) shows that attacks simply maximizing total variation score at the image level are less effective compared to *Poison-splat*, which highlights the crucial role of the proxy model in our attack design.

down training speed. This property would further strengthen the attack, since the overwhelming GPU occupancy will last longer than normal training may take, making the overall loss of computation power higher. As shown in the bottom of Table 1, if we do not put constraints on the attacker and let it modify the image pixels unlimitedly, then the attack results would be even more damaging. For instance, in the NeRF-Synthetic (ship) scene, **the peak GPU usage could increase up to 21 times and almost reach 80 GB GPU memory**. This level approaches the upper limits of the most advanced GPUs currently available, such as H100 and A100, and is undeniably destructive.



(a) Evolution of the proxy model in an ϵ -constrained attack



(b) Evolution of the proxy model in an unconstrained attack

Figure 4: Visualizations of proxy model updates during an attack process. The proxy 3DGS model gradually obtains more complexity from learning from non-smoothness in the 2D image space.

To help the readers build more understanding into the attack procedure, we visualize the internal states during the attack optimization procedure, rendering the proxy model in Figure 4. It is evident that the proxy model can be guided from non-smoothness of 2D images to develop highly complex

Table 1: Attack results of *Poison-splat* across multiple datasets. Constrained attacks ($\epsilon = 16/255$) can covertly increase training costs through minor perturbations to images. In contrast, unconstrained attacks allow for unlimited modifications to the original input, leading to significantly higher resource consumption and more extensive damage. We highlight attacks which successfully consume over **24 GB GPU memory**, which can cause a denial-of-service (*i.e.*, out-of-memory error and service halting) if 3DGS service is provided on a common 24GB-memory GPU (*e.g.*, RTX 3090, RTX 4090 or A5000). Full results on all scenes provided in Table 3 and Table 4.

Constrained Poison-splat attack with $\epsilon = 16/255$									
Metric	Number of Gaussians		Peak GPU memory [MB]		Training time [minutes]		Render speed [FPS]		
Setting \ Scene	clean	poisoned	clean	poisoned	clean	poisoned	clean	poisoned	
NS-hotdog	0.185 M	1.147 M (6.20x \uparrow)	3336	29747* (8.92x \uparrow)	8.57	17.43 (2.03x \uparrow)	443	69 (6.42x \downarrow)	
NS-lego	0.341 M	0.805 M (2.36x \uparrow)	3532	9960 (2.82x \uparrow)	8.62	13.02 (1.51x \uparrow)	349	145 (2.41x \downarrow)	
NS-materials	0.169 M	0.410 M (2.43x \uparrow)	3172	4886 (1.54x \uparrow)	7.33	9.92 (1.35x \uparrow)	447	250 (1.79x \downarrow)	
NS-ship	0.272 M	1.071 M (3.94x \uparrow)	3692	16666 (4.51x \uparrow)	8.87	16.12 (1.82x \uparrow)	326	87 (3.75x \downarrow)	
TT-Courthouse	0.604 M	0.733 M (1.21x \uparrow)	11402	12688 (1.11x \uparrow)	13.81	14.49 (1.05x \uparrow)	284	220 (1.29x \downarrow)	
TT-Courtroom	2.890 M	5.450 M (1.89x \uparrow)	9896	16308 (1.65x \uparrow)	16.88	23.92 (1.42x \uparrow)	139	83 (1.67x \downarrow)	
TT-Museum	4.439 M	7.130 M (1.61x \uparrow)	12704	18790 (1.48x \uparrow)	19.79	26.38 (1.33x \uparrow)	121	78 (1.55x \downarrow)	
TT-Playground	2.309 M	4.307 M (1.87x \uparrow)	8717	13032 (1.50x \uparrow)	15.17	21.82 (1.44x \uparrow)	151	87 (1.74x \downarrow)	
MIP-bicycle	5.793 M	10.129 M (1.75x \uparrow)	17748	27074* (1.53x \uparrow)	33.42	44.44 (1.33x \uparrow)	69	43 (1.60x \downarrow)	
MIP-counter	1.195 M	4.628 M (3.87x \uparrow)	10750	29796* (2.77x \uparrow)	26.46	37.63 (1.42x \uparrow)	164	51 (3.22x \downarrow)	
MIP-room	1.513 M	7.129 M (4.71x \uparrow)	12316	46238* (3.75x \uparrow)	25.36	47.98 (1.89x \uparrow)	154	35 (4.40x \downarrow)	
MIP-stump	4.671 M	10.003 M (2.14x \uparrow)	14135	25714* (1.82x \uparrow)	27.06	38.48 (1.42x \uparrow)	111	57 (1.95x \downarrow)	
Unconstrained Poison-splat attack with $\epsilon = \infty$									
Metric	Number of Gaussians		Peak GPU memory [MB]		Training time [minutes]		Render speed [FPS]		
Setting \ Scene	clean	poisoned	clean	poisoned	clean	poisoned	clean	poisoned	
NS-hotdog	0.185 M	4.272 M (23.09x \uparrow)	3336	47859* (14.35x \uparrow)	8.57	38.85 (4.53x \uparrow)	443	29 (15.28x \downarrow)	
NS-lego	0.341 M	4.159 M (12.20x \uparrow)	3532	78852* (22.33x \uparrow)	8.62	42.46 (4.93x \uparrow)	349	25 (13.96x \downarrow)	
NS-mic	0.205 M	3.940 M (19.22x \uparrow)	3499	61835* (17.67x \uparrow)	8.08	39.02 (4.83x \uparrow)	300	29 (10.34x \downarrow)	
NS-ship	0.272 M	4.317 M (15.87x \uparrow)	3692	80956* (21.93x \uparrow)	8.87	44.11 (4.97x \uparrow)	326	24 (13.58x \downarrow)	
TT-Courthouse	0.604 M	3.388 M (5.61x \uparrow)	11402	29856* (2.62x \uparrow)	13.81	25.33 (1.83x \uparrow)	284	54 (5.26x \downarrow)	
TT-Courtroom	2.890 M	13.196 M (4.57x \uparrow)	9896	33871* (3.42x \uparrow)	16.88	41.69 (2.47x \uparrow)	139	41 (3.39x \downarrow)	
TT-Museum	4.439 M	16.501 M (3.72x \uparrow)	12704	43317* (3.41x \uparrow)	19.79	48.89 (2.47x \uparrow)	121	36 (3.36x \downarrow)	
TT-Playground	2.309 M	10.306 M (4.46x \uparrow)	8717	27304* (3.13x \uparrow)	15.17	38.77 (2.56x \uparrow)	151	39 (3.87x \downarrow)	
MIP-bicycle	5.793 M	25.268 M (4.36x \uparrow)	17748	63236* (3.56x \uparrow)	33.42	81.48 (2.44x \uparrow)	69	16 (4.31x \downarrow)	
MIP-counter	1.195 M	11.167 M (9.34x \uparrow)	10750	80732* (7.51x \uparrow)	26.46	62.04 (2.34x \uparrow)	164	19 (8.63x \downarrow)	
MIP-room	1.513 M	16.019 M (10.59x \uparrow)	12316	57540* (4.67x \uparrow)	25.36	76.25 (3.01x \uparrow)	154	17 (9.06x \downarrow)	
MIP-stump	4.671 M	13.550 M (2.90x \uparrow)	14135	36181* (2.56x \uparrow)	27.06	51.51 (1.90x \uparrow)	111	27 (4.11x \downarrow)	

3D shapes. Consequently, the poisoned data produced from the projection of this over-densified proxy model can produce more poisoned data, inducing more Gaussians to fit these poisoned data.

4.2 BLACK-BOX ATTACK PERFORMANCE

The attack results described previously assume a white-box scenario, where the attacker is fully aware of the victim system’s details. In real-world, companies may utilize proprietary algorithms of their own, where the attacker may have no knowledge about their hyper-parameter settings or even their underlying 3DGS representations. This raises an important question: Can *Poison-splat* remain effective against black-box victim systems?

The answer is affirmative. To test the effectiveness of our attack on a black-box victim, we chose Scaffold-GS (Lu et al., 2024), a 3DGS variant algorithm designed with a focus on efficiency. Scaffold-GS differs significantly from traditional Gaussian Splatting as it utilizes anchor points to distribute local 3D Gaussians, which greatly alters the underlying feature representation. We directly tested Scaffold-GS on the poisoned dataset we crafted for the traditional 3DGS algorithm, making the victim (Scaffold-GS trainer) a black-box model. The results, as presented in Table 2 and Table 5, demonstrate the attack’s capability to generalize effectively, as evidenced by increased Gaussian parameters, higher GPU memory consumption, and reduced training speed.

The key reason for the success of generalization ability to black-box victims is our core intuition: promoting the non-smoothness of input images while maintaining their 3D consistency. This approach

Table 2: Black-box attack results on NeRF-Synthetic and MIP-NeRF360 dataset. The victim system, Scaffold-GS, utilizes distinctly different Gaussian Splatting feature representations compared to traditional Gaussian Splatting and remains unknown to the attacker. These results demonstrate the robust generalization ability of our attack against unknown black-box victim systems. Full results provided in Table 5.

Metric \ Scene	Number of Gaussians		Peak GPU memory [MB]		Training time [minutes]		
	clean	poisoned	clean	poisoned	clean	poisoned	
Constrained Black-box Poison-splat attack with $\epsilon = 16/255$ against Scaffold-GS							
NS-lego	0.414 M	2.074 M (5.01x \uparrow)	3003	4808 (1.60x \uparrow)	9.77	17.91 (1.83x \uparrow)	
NS-ship	1.000 M	3.291 M (3.29x \uparrow)	3492	5024 (1.44x \uparrow)	11.68	21.92 (1.88x \uparrow)	
MIP-bonsai	4.368 M	10.608 M (2.43x \uparrow)	10080	12218 (1.21x \uparrow)	35.33	37.71 (1.07x \uparrow)	
MIP-stump	6.798 M	14.544 M (2.14x \uparrow)	7322	9432 (1.29x \uparrow)	33.53	36.32 (1.08x \uparrow)	
Unconstrained Black-box Poison-splat attack with $\epsilon = \infty$ against Scaffold-GS							
NS-lego	0.414 M	3.973 M (9.60x \uparrow)	3003	6242 (2.08x \uparrow)	9.77	26.11 (2.67x \uparrow)	
NS-ship	1.000 M	4.717 M (4.72x \uparrow)	3492	6802 (1.95x \uparrow)	11.68	28.22 (2.42x \uparrow)	
MIP-bonsai	4.368 M	28.042 M (6.42x \uparrow)	10080	22115 (2.19x \uparrow)	35.33	78.36 (2.22x \uparrow)	
MIP-stump	6.798 M	34.027 M (5.01x \uparrow)	7322	20797 (2.84x \uparrow)	33.53	79.64 (2.38x \uparrow)	

ensures that our poisoned dataset effectively increases the number of 3D-representation units for all adaptive complexity 3D reconstruction algorithms, regardless of the specific algorithm used.

4.3 ABLATION STUDY ON PROXY MODEL

We next ablate the effectiveness of our proxy model. As shown in Figure 3(b), we compare the number of Gaussians produced in victim learning procedures with two baselines: the green curve represents trajectory training on clean data, and the yellow curve represents a naive Total Variation maximizing attack, which does not involve a proxy model, but only maximize Total Variation score on each view individually. As we show in Figure 3(b), this naive attack is not as effective as our attack design. We attribute this reason to be lack of consistency of multi-view information. Since the Total Variation loss is a local image operator, individually maximizing the TV loss on each image will result in a noised dataset without aligning with each other. As a result, victim learning from this noised set of images struggles to align shapes in 3D space, and the training on fine details becomes harder to converge. Thus, when faced with conflicting textures from different views, the Gaussian Splatting technique fails to effectively perform reconstruction on details, leading to fewer Gaussians produced compared with our attack. We use this study to highlight the necessity of decoy model in our attack methodology design.

4.4 DISCUSSIONS ON NAIVE DEFENSE STRATEGIES

Our attack method maximizes the computational costs of 3DGS by optimizing the number of Gaussians. One may argue that a straightforward defense method is to simply impose an upper limit on the number of Gaussians during victim training to thwart the attack. However, such a straightforward strategy is not as effective as expected. While limiting the number of Gaussians might mitigate the direct impact on computational costs, it significantly degrades the quality of 3D reconstruction, as demonstrated in Figure 5. The figure shows that 3DGS models trained under these defensive constraints perform much worse compared to those with unconstrained training, particularly in terms of detail reconstruction. This decline in quality occurs because **3DGS cannot automatically distinguish necessary fine details from poisoned textures**. Naively capping the number of Gaussians will directly lead to the failure of the model to reconstruct the 3D scene accurately, which violates the primary goal of the service provider. This study demonstrates more sophisticated defensive strategies are necessary to both protect the system and maintain the quality of 3D reconstructions under our attack.



Figure 5: *Poison-splat* attack cannot be painlessly defended by simply constraining the number of Gaussians during 3DGS optimization. As demonstrated, while this defense can cap the maximum resource consumption, it markedly degrades the quality of 3D reconstruction, in terms of photo-realism and fine-grained details of the rendered images, which violates the primary goal of the service provider.

5 CONCLUSION AND DISCUSSIONS

This paper uncovers a significant yet previously overlooked security vulnerability in 3D Gaussian Splatting (3DGS). To this end, we have proposed a novel *Poison-splat* attack method, which dramatically escalates the computational demands of 3DGS and can even trigger a Denial-of-Service (*e.g.*, server disruption), causing substantial financial losses for 3DGS service providers. By leveraging a sophisticated bi-level optimization framework and strategies such as attack objective approximation, proxy model rendering, and optional constrained optimization, we demonstrate the feasibility of such attacks and emphasize the challenges in countering them with naive defenses. To the best of our knowledge, this is the first research work to explore an attack on 3DGS, and the first attack targeting the computation complexity of training phase in machine learning systems. We encourage researchers and practitioners in the field of 3DGS to acknowledge this security vulnerability and work together towards more robust algorithms and defense strategies against such threats. Lastly, we would like to discuss potential limitations, future directions, and social impacts of our work.

Limitations and Future directions. There are still limitations of our work, and we expect future studies can work on them:

- Better approximation of outer maximum optimization.** In this work, we approximate the outer maximum objective (*i.e.*, the computational cost) with the number of Gaussians. Although the number of Gaussians strongly correlates with GPU memory occupancy and rendering latency, there could be better optimizable metrics for this purpose. For example, the "density" of Gaussians, *i.e.*, the number of Gaussians falling into the same tile to involve in alpha-blending, might be a better metric to achieve better optimization outcomes.
- Better defense methods.** We focus on developing attack methods, without delving deeply into defensive strategies. We hope future studies can propose more robust 3DGS algorithms or develop more effective defensive techniques to counteract such attacks. This focus could significantly enhance the security and reliability of 3DGS systems in practical applications.

Societal Impacts. While our methods could potentially be misused by malicious actors to disrupt 3DGS service providers and cause financial harm, our aim is not to facilitate such actions. Instead, our objective is to highlight significant security vulnerabilities within 3DGS systems and prompt the community—researchers, practitioners, and providers—to recognize and address these gaps. We aim to inspire the development of more robust algorithms and defensive strategies, enhancing the security and reliability of 3DGS systems in practical applications. We are committed to ethical research and do not endorse using our findings to inflict societal harm.

REFERENCES

- 540
541
542 Pandey Akash. Midjourney bans stability ai from using its service: Here’s why.
543 [https://www.newsbytesapp.com/news/science/midjourney-bans-stability-ai-workers-over-](https://www.newsbytesapp.com/news/science/midjourney-bans-stability-ai-workers-over-alleged-data-scraping/story)
544 [alleged-data-scraping/story](https://www.newsbytesapp.com/news/science/midjourney-bans-stability-ai-workers-over-alleged-data-scraping/story), 2024.
- 545 Theyazn HH Aldhyani and Hasan Alkahtani. Cyber security for detecting distributed denial of service
546 attacks in agriculture 4.0: Deep learning model. *Mathematics*, 11(1):233, 2023.
- 547
548 Marco Barreno, Blaine Nelson, Anthony D Joseph, and J Doug Tygar. The security of machine
549 learning. *Machine Learning*, 81:121–148, 2010.
- 550
551 Jonathan T Barron, Ben Mildenhall, Dor Verbin, Pratul P Srinivasan, and Peter Hedman. Mip-nerf
552 360: Unbounded anti-aliased neural radiance fields. In *Proceedings of the IEEE/CVF Conference*
553 *on Computer Vision and Pattern Recognition*, pp. 5470–5479, 2022.
- 554 Sajal Bhatia, Sunny Behal, and Irfan Ahmed. Distributed denial of service attacks and defense
555 mechanisms: current landscape and future directions. *Versatile Cybersecurity*, pp. 55–97, 2018.
- 556
557 Battista Biggio, Blaine Nelson, and Pavel Laskov. Poisoning attacks against support vector machines.
558 In *Proceedings of the 29th International Conference on International Conference on Machine*
559 *Learning*, pp. 1467–1474, 2012.
- 560
561 Battista Biggio, Iginio Corona, Davide Maiorca, Blaine Nelson, Nedim Šrđić, Pavel Laskov, Giorgio
562 Giacinto, and Fabio Roli. Evasion attacks against machine learning at test time. In *Machine*
563 *Learning and Knowledge Discovery in Databases: European Conference, ECML PKDD 2013,*
564 *Prague, Czech Republic, September 23-27, 2013, Proceedings, Part III 13*, pp. 387–402. Springer,
2013.
- 565
566 Dominique Brunet, Edward R Vrscay, and Zhou Wang. On the mathematical properties of the
567 structural similarity index. *IEEE Transactions on Image Processing*, 21(4):1488–1499, 2011.
- 568
569 Samuel Rota Bulò, Lorenzo Porzi, and Peter Kotschieder. Revising densification in gaussian
570 splatting. *arXiv preprint arXiv:2404.06109*, 2024.
- 571
572 Nicholas Carlini, Florian Tramer, Eric Wallace, Matthew Jagielski, Ariel Herbert-Voss, Katherine
573 Lee, Adam Roberts, Tom Brown, Dawn Song, Ulfar Erlingsson, et al. Extracting training data
574 from large language models. In *30th USENIX Security Symposium (USENIX Security 21)*, pp.
2633–2650, 2021.
- 575
576 Nicolas Carlini, Jamie Hayes, Milad Nasr, Matthew Jagielski, Vikash Sehwal, Florian Tramer, Borja
577 Balle, Daphne Ippolito, and Eric Wallace. Extracting training data from diffusion models. In *32nd*
578 *USENIX Security Symposium (USENIX Security 23)*, pp. 5253–5270, 2023.
- 579
580 Anirban Chakraborty, Manaar Alam, Vishal Dey, Anupam Chattopadhyay, and Debdeep Mukhopad-
hyay. Adversarial attacks and defences: A survey. *arXiv preprint arXiv:1810.00069*, 2018.
- 581
582 Varun Chandrasekaran, Kamalika Chaudhuri, Irene Giacomelli, Somesh Jha, and Songbai Yan.
583 Exploring connections between active learning and model extraction. In *29th USENIX Security*
584 *Symposium (USENIX Security 20)*, pp. 1309–1326, 2020.
- 585
586 Guikun Chen and Wenguan Wang. A survey on 3d gaussian splatting. *arXiv preprint*
arXiv:2401.03890, 2024.
- 587
588 Simin Chen, Cong Liu, Mirazul Haque, Zihe Song, and Wei Yang. Nmtslowdown: understanding and
589 testing efficiency degradation of neural machine translation systems. In *Proceedings of the 30th*
590 *ACM Joint European Software Engineering Conference and Symposium on the Foundations of*
591 *Software Engineering*, pp. 1148–1160, 2022a.
- 592
593 Simin Chen, Zihe Song, Mirazul Haque, Cong Liu, and Wei Yang. Nicslowdown: Evaluating the
efficiency robustness of neural image caption generation models. In *Proceedings of the IEEE/CVF*
Conference on Computer Vision and Pattern Recognition, pp. 15365–15374, 2022b.

- 594 Simin Chen, Hanlin Chen, Mirazul Haque, Cong Liu, and Wei Yang. The dark side of dynamic
595 routing neural networks: Towards efficiency backdoor injection. In *Proceedings of the IEEE/CVF*
596 *Conference on Computer Vision and Pattern Recognition*, pp. 24585–24594, 2023.
- 597 Zilong Chen, Feng Wang, and Huaping Liu. Text-to-3d using gaussian splatting. In *CVPR*, 2024.
- 599 Kai Cheng, Xiaoxiao Long, Kaizhi Yang, Yao Yao, Wei Yin, Yuexin Ma, Wenping Wang, and
600 Xuejin Chen. Gaussianpro: 3d gaussian splatting with progressive propagation. *arXiv preprint*
601 *arXiv:2402.14650*, 2024.
- 602 Christopher A Choquette-Choo, Florian Tramer, Nicholas Carlini, and Nicolas Papernot. Label-only
603 membership inference attacks. In *International conference on machine learning*, pp. 1964–1974.
604 PMLR, 2021.
- 606 Anurag Dalal, Daniel Hagen, Kjell G Robbersmyr, and Kristian Muri Knausgård. Gaussian splatting:
607 3d reconstruction and novel view synthesis, a review. *arXiv preprint arXiv:2405.03417*, 2024.
- 608 Yinpeng Dong, Fangzhou Liao, Tianyu Pang, Hang Su, Jun Zhu, Xiaolin Hu, and Jianguo Li. Boosting
609 adversarial attacks with momentum. In *Proceedings of the IEEE conference on computer vision*
610 *and pattern recognition*, pp. 9185–9193, 2018.
- 611 Yinpeng Dong, Tianyu Pang, Hang Su, and Jun Zhu. Evading defenses to transferable adversarial ex-
612 amples by translation-invariant attacks. In *Proceedings of the IEEE/CVF Conference on Computer*
613 *Vision and Pattern Recognition*, pp. 4312–4321, 2019.
- 615 Khaled M Elleithy, Drazen Blagovic, Wang K Cheng, and Paul Sideleau. Denial of service attack
616 techniques: analysis, implementation and comparison. 2005.
- 617 Guangchi Fang and Bing Wang. Mini-splatting: Representing scenes with a constrained number of
618 gaussians. *arXiv preprint arXiv:2403.14166*, 2024.
- 620 Ben Fei, Jingyi Xu, Rui Zhang, Qingyuan Zhou, Weidong Yang, and Ying He. 3d gaussian as a new
621 vision era: A survey. *arXiv preprint arXiv:2402.07181*, 2024.
- 622 Liam Fowl, Ping-yeh Chiang, Micah Goldblum, Jonas Geiping, Arpit Bansal, Wojtek Czaja, and Tom
623 Goldstein. Preventing unauthorized use of proprietary data: Poisoning for secure dataset release.
624 *arXiv preprint arXiv:2103.02683*, 2021a.
- 625 Liam Fowl, Micah Goldblum, Ping-yeh Chiang, Jonas Geiping, Wojciech Czaja, and Tom Goldstein.
626 Adversarial examples make strong poisons. *Advances in Neural Information Processing Systems*,
627 34:30339–30351, 2021b.
- 629 Matt Fredrikson, Somesh Jha, and Thomas Ristenpart. Model inversion attacks that exploit confidence
630 information and basic countermeasures. In *Proceedings of the 22nd ACM SIGSAC conference on*
631 *computer and communications security*, pp. 1322–1333, 2015.
- 632 Yonggan Fu, Ye Yuan, Souvik Kundu, Shang Wu, Shun Yao Zhang, and Yingyan Lin. Nerfool: Un-
633 covering the vulnerability of generalizable neural radiance fields against adversarial perturbations.
634 In *Proceedings of the 30th International Conference on Machine Learning, ICML 2013*, 2023.
- 635 Kuofeng Gao, Yang Bai, Jindong Gu, Shu-Tao Xia, Philip Torr, Zhifeng Li, and Wei Liu. Induc-
636 ing high energy-latency of large vision-language models with verbose images. In *The Twelfth*
637 *International Conference on Learning Representations*, 2023.
- 639 Jonas Geiping, Hartmut Bauermeister, Hannah Dröge, and Michael Moeller. Inverting gradients-how
640 easy is it to break privacy in federated learning? *Advances in Neural Information Processing*
641 *Systems*, 33:16937–16947, 2020.
- 642 Google. Google announces new google maps experience featuring neural radiance fields
643 (nerfs). [https://radiancefields.com/google-announces-new-google-maps-experience-featuring-](https://radiancefields.com/google-announces-new-google-maps-experience-featuring-neural-radiance-fields/)
644 [neural-radiance-fields/](https://radiancefields.com/google-announces-new-google-maps-experience-featuring-neural-radiance-fields/), 2023.
- 645 Sanghyun Hong, Yiğitcan Kaya, Ionuț-Vlad Modoranu, and Tudor Dumitraș. A panda? no, it’s
646 a sloth: Slowdown attacks on adaptive multi-exit neural network inference. *arXiv preprint*
647 *arXiv:2010.02432*, 2020.

- 648 András Horváth and Csaba M Józsa. Targeted adversarial attacks on generalizable neural radiance
649 fields. In *Proceedings of the IEEE/CVF International Conference on Computer Vision*, pp. 3718–
650 3727, 2023.
- 651 W Ronny Huang, Jonas Geiping, Liam Fowl, Gavin Taylor, and Tom Goldstein. Metapoison: Practical
652 general-purpose clean-label data poisoning. *Advances in Neural Information Processing Systems*,
653 33:12080–12091, 2020.
- 654 Matthew Jagielski, Alina Oprea, Battista Biggio, Chang Liu, Cristina Nita-Rotaru, and Bo Li.
655 Manipulating machine learning: Poisoning attacks and countermeasures for regression learning. In
656 *2018 IEEE symposium on security and privacy (SP)*, pp. 19–35. IEEE, 2018.
- 657 Nikhil Keetha, Jay Karhade, Krishna Murthy Jatavallabhula, Gengshan Yang, Sebastian Scherer,
658 Deva Ramanan, and Jonathon Luiten. Splatam: Splat, track and map 3d gaussians for dense rgb-d
659 slam. In *Proceedings of the IEEE/CVF Conference on Computer Vision and Pattern Recognition*,
660 2024.
- 661 Bernhard Kerbl, Georgios Kopanas, Thomas Leimkühler, and George Drettakis. 3d gaussian splatting
662 for real-time radiance field rendering. *ACM SIGGRAPH*, 42(4), 2023.
- 663 KIRI. Kiri engine app. [https://www.kiriengine.app/blog/3d-gaussian-splatting-editing-on-
664 smartphones-for-the-first-time](https://www.kiriengine.app/blog/3d-gaussian-splatting-editing-on-smartphones-for-the-first-time).
- 665 Arno Knapitsch, Jaesik Park, Qian-Yi Zhou, and Vladlen Koltun. Tanks and temples: Benchmarking
666 large-scale scene reconstruction. *ACM Transactions on Graphics*, 36(4), 2017.
- 667 Muhammed Kocabas, Jen-Hao Rick Chang, James Gabriel, Oncel Tuzel, and Anurag Ranjan. HUGS:
668 Human gaussian splatting. In *2024 IEEE/CVF Conference on Computer Vision and Pattern
669 Recognition (CVPR)*, 2024. URL <https://arxiv.org/abs/2311.17910>.
- 670 Pang Wei Koh and Percy Liang. Understanding black-box predictions via influence functions. In
671 *International conference on machine learning*, pp. 1885–1894. PMLR, 2017.
- 672 Pang Wei Koh, Jacob Steinhardt, and Percy Liang. Stronger data poisoning attacks break data
673 sanitization defenses. *Machine Learning*, pp. 1–47, 2022.
- 674 Jiahui Lei, Yufu Wang, Georgios Pavlakos, Lingjie Liu, and Kostas Daniilidis. Gart: Gaussian
675 articulated template models. In *2024 IEEE/CVF Conference on Computer Vision and Pattern
676 Recognition (CVPR)*, 2024. URL <https://arxiv.org/abs/2311.16099>.
- 677 Bo Li, Yining Wang, Aarti Singh, and Yevgeniy Vorobeychik. Data poisoning attacks on factorization-
678 based collaborative filtering. *Advances in neural information processing systems*, 29, 2016.
- 679 Yanyan Li, Chenyu Lyu, Yan Di, Guangyao Zhai, Gim Hee Lee, and Federico Tombari. Geogaussian:
680 Geometry-aware gaussian splatting for scene rendering. *arXiv preprint arXiv:2403.11324*, 2024.
- 681 Neil Long and Rob Thomas. Trends in denial of service attack technology. *CERT Coordination
682 Center*, 648(651):569, 2001.
- 683 Jiahao Lu, Xi Sheryl Zhang, Tianli Zhao, Xiangyu He, and Jian Cheng. April: Finding the achilles’
684 heel on privacy for vision transformers. In *Proceedings of the IEEE/CVF Conference on Computer
685 Vision and Pattern Recognition*, pp. 10051–10060, 2022.
- 686 Tao Lu, Mulin Yu, Linning Xu, Yuanbo Xiangli, Limin Wang, Dahua Lin, and Bo Dai. Scaffold-gs:
687 Structured 3d gaussians for view-adaptive rendering. In *Proceedings of the IEEE/CVF Conference
688 on Computer Vision and Pattern Recognition*, pp. 20654–20664, 2024.
- 689 Jonathon Luiten, Georgios Kopanas, Bastian Leibe, and Deva Ramanan. Dynamic 3d gaussians:
690 Tracking by persistent dynamic view synthesis. In *3DV*, 2024.
- 691 LumaAI. Luma ai. <https://lumalabs.ai/>.
- 692 Aleksander Madry, Aleksandar Makelov, Ludwig Schmidt, Dimitris Tsipras, and Adrian Vladu.
693 Towards deep learning models resistant to adversarial attacks. In *International Conference on
694 Learning Representations*, 2018.

- 702 Hidenobu Matsuki, Riku Murai, Paul H. J. Kelly, and Andrew J. Davison. Gaussian Splatting SLAM.
703 In *Proceedings of the IEEE/CVF Conference on Computer Vision and Pattern Recognition*, 2024.
704
- 705 Shike Mei and Xiaojin Zhu. The security of latent dirichlet allocation. In *Artificial Intelligence and*
706 *Statistics*, pp. 681–689. PMLR, 2015a.
- 707 Shike Mei and Xiaojin Zhu. Using machine teaching to identify optimal training-set attacks on
708 machine learners. In *Proceedings of the aaii conference on artificial intelligence*, volume 29,
709 2015b.
- 710
- 711 Ben Mildenhall, Pratul P Srinivasan, Matthew Tancik, Jonathan T Barron, Ravi Ramamoorthi, and
712 Ren Ng. Nerf: Representing scenes as neural radiance fields for view synthesis. *Communications*
713 *of the ACM*, 65(1):99–106, 2021.
- 714 Jelena Mirkovic and Peter Reiher. A taxonomy of ddos attack and ddos defense mechanisms. *ACM*
715 *SIGCOMM Computer Communication Review*, 34(2):39–53, 2004.
716
- 717 Luis Muñoz-González, Battista Biggio, Ambra Demontis, Andrea Paudice, Vasin Wongrassamee,
718 Emil C Lupu, and Fabio Roli. Towards poisoning of deep learning algorithms with back-gradient
719 optimization. In *Proceedings of the 10th ACM workshop on artificial intelligence and security*, pp.
720 27–38, 2017.
- 721 Daryna Oliynyk, Rudolf Mayer, and Andreas Rauber. I know what you trained last summer: A survey
722 on stealing machine learning models and defences. *ACM Computing Surveys*, 2023.
723
- 724 Nikolaos Pitropakis, Emmanouil Panaousis, Thanassis Giannetsos, Eleftherios Anastasiadis, and
725 George Loukas. A taxonomy and survey of attacks against machine learning. *Computer Science*
726 *Review*, 34:100199, 2019.
- 727 Polycam. Polycam. <https://poly.cam/pricing>.
728
- 729 Maria Rigaki and Sebastian Garcia. A survey of privacy attacks in machine learning. *ACM Computing*
730 *Surveys*, 56(4):1–34, 2023.
- 731 Leonid I Rudin, Stanley Osher, and Emad Fatemi. Nonlinear total variation based noise removal
732 algorithms. *Physica D: nonlinear phenomena*, 60(1-4):259–268, 1992.
733
- 734 Ahmed Salem, Yang Zhang, Mathias Humbert, Mario Fritz, and Michael Backes. MI-leaks: Model
735 and data independent membership inference attacks and defenses on machine learning models. In
736 *Network and Distributed Systems Security Symposium 2019*. Internet Society, 2019.
- 737 Qihong Shen, Xuanyu Yi, Zike Wu, Pan Zhou, Hanwang Zhang, Shuicheng Yan, and Xinchao Wang.
738 Gamba: Marry gaussian splatting with mamba for single view 3d reconstruction. *arXiv preprint*
739 *arXiv:2403.18795*, 2024.
740
- 741 Reza Shokri, Marco Stronati, Congzheng Song, and Vitaly Shmatikov. Membership inference attacks
742 against machine learning models. In *2017 IEEE symposium on security and privacy (SP)*, pp. 3–18.
743 IEEE, 2017.
- 744 Ilia Shumailov, Yiren Zhao, Daniel Bates, Nicolas Papernot, Robert Mullins, and Ross Anderson.
745 Sponge examples: Energy-latency attacks on neural networks. In *2021 IEEE European symposium*
746 *on security and privacy (EuroS&P)*, pp. 212–231. IEEE, 2021.
747
- 748 Spline. Spline. <https://spline.design/pricing>.
749
- 750 Christian Szegedy, Wojciech Zaremba, Ilya Sutskever, Joan Bruna, Dumitru Erhan, Ian Goodfellow,
751 and Rob Fergus. Intriguing properties of neural networks. *arXiv preprint arXiv:1312.6199*, 2013.
- 752 Jiaxiang Tang, Jiawei Ren, Hang Zhou, Ziwei Liu, and Gang Zeng. Dreamgaussian: Generative
753 gaussian splatting for efficient 3d content creation. In *ICLR*, 2024.
754
- 755 Zhiyi Tian, Lei Cui, Jie Liang, and Shui Yu. A comprehensive survey on poisoning attacks and
countermeasures in machine learning. *ACM Computing Surveys*, 55(8):1–35, 2022.

- 756 Carlo Tomasi and Roberto Manduchi. Bilateral filtering for gray and color images. In *Sixth*
757 *international conference on computer vision (IEEE Cat. No. 98CH36271)*, pp. 839–846. IEEE,
758 1998.
- 759 Florian Tramèr, Fan Zhang, Ari Juels, Michael K Reiter, and Thomas Ristenpart. Stealing machine
760 learning models via prediction {APIs}. In *25th USENIX security symposium (USENIX Security*
761 *16)*, pp. 601–618, 2016.
- 762 Shizun Wang, Xingyi Yang, Qihong Shen, Zhenxiang Jiang, and Xinchao Wang. Gflow: Recovering
763 4d world from monocular video. *arXiv preprint arXiv:2405.18426*, 2024a.
- 764 Yuxuan Wang, Xuanyu Yi, Zike Wu, Na Zhao, Long Chen, and Hanwang Zhang. View-consistent 3d
765 editing with gaussian splatting. *arXiv preprint arXiv:2403.11868*, 2024b.
- 766 Guanjun Wu, Taoran Yi, Jiemin Fang, Lingxi Xie, Xiaopeng Zhang, Wei Wei, Wenyu Liu, Qi Tian,
767 and Wang Xinggang. 4d gaussian splatting for real-time dynamic scene rendering. In *CVPR*,
768 2024a.
- 769 Tong Wu, Yu-Jie Yuan, Ling-Xiao Zhang, Jie Yang, Yan-Pei Cao, Ling-Qi Yan, and Lin Gao. Recent
770 advances in 3d gaussian splatting. *arXiv preprint arXiv:2403.11134*, 2024b.
- 771 Shaoyuan Xie, Zichao Li, Zeyu Wang, and Cihang Xie. On the adversarial robustness of camera-based
772 3d object detection. *Transactions on Machine Learning Research*, 2024a.
- 773 Tianyi Xie, Zeshun Zong, Yuxing Qiu, Xuan Li, Yutao Feng, Yin Yang, and Chenfanfu Jiang.
774 Physgaussian: Physics-integrated 3d gaussians for generative dynamics. In *CVPR*, 2024b.
- 775 Chi Yan, Delin Qu, Dan Xu, Bin Zhao, Zhigang Wang, Dong Wang, and Xuelong Li. Gs-slam: Dense
776 visual slam with 3d gaussian splatting. In *CVPR*, 2024a.
- 777 Zhiwen Yan, Weng Fei Low, Yu Chen, and Gim Hee Lee. Multi-scale 3d gaussian splatting for
778 anti-aliased rendering. In *Proceedings of the IEEE/CVF Conference on Computer Vision and*
779 *Pattern Recognition*, pp. 20923–20931, 2024b.
- 780 Zeyu Yang, Hongye Yang, Zijie Pan, and Li Zhang. Real-time photorealistic dynamic scene rep-
781 resentation and rendering with 4d gaussian splatting. In *International Conference on Learning*
782 *Representations (ICLR)*, 2024.
- 783 Mingqiao Ye, Martin Danelljan, Fisher Yu, and Lei Ke. Gaussian grouping: Segment and edit
784 anything in 3d scenes. *arXiv preprint arXiv:2312.00732*, 2023.
- 785 Zongxin Ye, Wenyu Li, Sidun Liu, Peng Qiao, and Yong Dou. Absgs: Recovering fine details for 3d
786 gaussian splatting. *arXiv preprint arXiv:2404.10484*, 2024.
- 787 Taoran Yi, Jiemin Fang, Junjie Wang, Guanjun Wu, Lingxi Xie, Xiaopeng Zhang, Wenyu Liu, Qi Tian,
788 and Xinggang Wang. Gaussiandreamer: Fast generation from text to 3d gaussians by bridging 2d
789 and 3d diffusion models. In *CVPR*, 2024.
- 790 Weichen Yu, Tianyu Pang, Qian Liu, Chao Du, Bingyi Kang, Yan Huang, Min Lin, and Shuicheng
791 Yan. Bag of tricks for training data extraction from language models. In *Proceedings of the 40th*
792 *International Conference on Machine Learning, ICML’23*. JMLR.org, 2023.
- 793 Zehao Yu, Anpei Chen, Binbin Huang, Torsten Sattler, and Andreas Geiger. Mip-splatting: Alias-free
794 3d gaussian splatting. In *Proceedings of the IEEE/CVF Conference on Computer Vision and*
795 *Pattern Recognition*, pp. 19447–19456, 2024.
- 796 Wojciech Zielonka, Timur Bagautdinov, Shunsuke Saito, Michael Zollhöfer, Justus Thies, and Javier
797 Romero. Drivable 3d gaussian avatars. *arXiv preprint arXiv:2311.08581*, 2023.
- 798
799
800
801
802
803
804
805
806
807
808
809

APPENDIX

The Appendix is organized as follows: Section A discusses related works; Section B provides a formal and comprehensive description of 3D Gaussian Splatting training. Section D offers the full results of experiments mentioned in the main paper, presented here due to page constraints. Section E lists all the notations used throughout the paper. Section F presents examples of attacker-crafted poisoned images and the corresponding reconstructions from victim models trained with those images.

A RELATED WORKS

A.1 3D GAUSSIAN SPLATTING

3D Gaussian Splatting is receiving overwhelming popularity in the 3D vision domain (Chen & Wang, 2024; Fei et al., 2024; Wu et al., 2024b; Dalal et al., 2024). The explicit nature of 3D Gaussian Splatting enables real-time rendering capabilities and unparalleled levels of control and editability, demonstrating its effectiveness in 3D generation. Since its introduction in (Kerbl et al., 2023), 3D Gaussian Splatting has facilitated a diverse array of downstream applications, including text-to-3D generation (Chen et al., 2024; Tang et al., 2024; Yi et al., 2024), Simultaneous Localization and Mapping (Keetha et al., 2024; Matsuki et al., 2024; Yan et al., 2024a), human avatars (Kocabas et al., 2024; Lei et al., 2024; Zielonka et al., 2023), 4D-dynamic scene modeling (Luiten et al., 2024; Wu et al., 2024a; Yang et al., 2024), and other applications (Xie et al., 2024b; Shen et al., 2024; Ye et al., 2023; Wang et al., 2024b;a).

While the majority of the audience in the 3D vision community places their focus on utility, we found only a handful of research works put efforts into investigating the security issues of 3D algorithms. Xie et al. (2024a) analyzed the resilience of 3D object detection systems under white-box and black-box attacks. (Fu et al., 2023; Horváth & Józsa, 2023) proposed attacks against Neural Radiance Fields (NeRFs). To our knowledge, this is the first attack ever proposed for 3D Gaussian Splatting systems.

A.2 ATTACKS ON MACHINE LEARNING SYSTEMS

Machine learning has been shown to be vulnerable to various types of attacks (Pitropakis et al., 2019; Rigaki & Garcia, 2023; Chakraborty et al., 2018; Oliynyk et al., 2023; Tian et al., 2022). The majority of attacks target the either *confidentiality* (including membership inference (Shokri et al., 2017; Salem et al., 2019; Choquette-Choo et al., 2021), data reconstruction attacks (Fredrikson et al., 2015; Carlini et al., 2021; 2023; Yu et al., 2023; Geiping et al., 2020; Lu et al., 2022) and model stealing attacks (Tramèr et al., 2016; Chandrasekaran et al., 2020)) or *integrity* (like adversarial attacks (Biggio et al., 2013; Szegedy et al., 2013; Dong et al., 2018; 2019) and data poisoning attacks (Barreno et al., 2010; Jagielski et al., 2018; Biggio et al., 2012; Mei & Zhu, 2015b)). Different from the above mentioned attacks, we aim to illustrate that by carefully crafting input images, the attacker can indeed attack *availability*, *i.e.*, timely and cost-affordable access to machine learning service. The most similar research is the work by Shumailov et al. (2021), which is the first Denial-of-Service (DoS) attack towards machine learning systems. It proposed sponge examples which can cause much more latency and energy consumption for language models and image classifiers, driving deep learning models to their worst performance. Different from the work (Shumailov et al., 2021), our attack targets 3D reconstruction algorithms and is not driven by neural networks.

A.2.1 DATA POISONING ATTACK

We consider our proposed attacks to fall into the category of data poisoning attack, which manipulates training data to launch the attack at the training stage. The attacker makes the first move to craft poisoned training samples, and the victim has a goal of training the system based on samples provided by the attacker. Solving this problem typically involves solving a max-min bi-level optimization problem, where the attacker wants to maximize some adversarial loss (*i.e.*, test error or computational cost) and victim wants to minimize the training objective (*i.e.*, training loss). Different literature solves the problem using different techniques (Biggio et al., 2012; Mei & Zhu, 2015b;a; Li et al., 2016). For many machine learning systems, given the inherent complexity and their reliance on large datasets, it is intractable to exactly do the bi-level optimization. The work (Muñoz-González et al., 2017) exploited back-gradient optimization technique to approximate real gradients through

reverse-mode differentiation. The work (Huang et al., 2020) formulated as a meta-learning problem, and approximated the inner optimal solution by training only K SGD steps for each outer objective evaluation. The work (Koh et al., 2022) proposed three methods to approximate the expensive bi-level optimization: influence functions (Koh & Liang, 2017), minimax duality and Karush-Kuhn-Tucker (KKT) conditions. The work (Fowl et al., 2021a) used gradient matching which assumes inner optimality has been achieved by a fixed model. The work (Fowl et al., 2021b) avoided the bi-level optimization with a well-trained proxy model from clean data. Different from these previous studies, we propose a gradient-free optimization process to solve the outer optimization pipeline, and show a good optimization result on the attacker’s goal.

A.2.2 ENERGY-LATENCY ATTACKS IN MACHINE LEARNING

A limited number of studies have investigated attacks to manipulate the computation cost needed for machine learning systems, mainly in inference-stage. Shumailov et al. (2021) initially brought people’s attention to sponge samples, which are malicious samples able to maximize the energy consumption and responsive latency of a neural network. Following this work, there are other works studying samples which can cause the worst case computation resource consumption in a (dynamic) machine learning systems, for example Hong et al. (2020) and Chen et al. (2023) found samples that can necessitate late exit in a dynamic-depth neural network. More up-to-date works utilize the flexible nature of language to attack NLP models, inducing extended natural language sequence responses to over-consume energy and latency (Chen et al., 2022b;a; Gao et al., 2023). However, to the best of our knowledge, there has been **no previous work targeting Denial-of-Service attacks at the training stage** of machine learning systems. Our work is pioneering in proposing a DoS attack specifically designed for the training phase of machine learning systems. Additionally, this is also the first effort to develop an attack against 3D Gaussian Splatting.

B MORE BACKGROUNDS OF 3D GAUSSIAN SPLATTING

3D Gaussian Splatting (3DGS) (Kerbl et al., 2023) has revolutionized the 3D vision community with its superior performance and efficiency. It models a 3D scene by learning a set of 3D Gaussians $\mathcal{G} = \{G_i\}$ from multi-view images $\mathcal{D} = \{V_k, P_k\}_{k=1}^N$, where each view consists of a ground-truth image V_k and the corresponding camera poses P_k . We denote N as the total number of image-pose pairs in the training data, which can be arbitrary and unfixed in 3DGS. As for the model, each 3D Gaussian $G_i = \{\mu_i, s_i, \alpha_i, q_i, c_i\}$ has 5 optimizable parameters: center coordinates $\mu_i \in \mathbb{R}^3$, scales $s_i \in \mathbb{R}^3$, opacity $\alpha_i \in \mathbb{R}$, rotation quaternion $q_i \in \mathbb{R}^4$, and associated view-dependent color represented as spherical harmonics $c_i \in \mathbb{R}^{3(d+1)^2}$, where d is the degree of spherical harmonics.

To render \mathcal{G} from 3D Gaussian space to 2D images, each Gaussian is first projected into the camera coordinate frame given a camera pose P_k to determine the depth of each Gaussian, which is the distance of that Gaussian to the camera view. The calculated depth is used for sorting Gaussians from near to far, and then the colors in 2D image are rendered in parallel by alpha blending according to the depth order of adjacent 3D Gaussians. The core reason for 3DGS to achieve real-time optimization and rendering lies in this tile-based differentiable rasterization pipeline. We denote the 3DGS renderer as a function \mathcal{R} , which takes as input the Gaussians \mathcal{G} and a camera pose P_k to render an image $V'_k = \mathcal{R}(\mathcal{G}, P_k)$.

The training is done by optimizing the reconstruction loss between the rendered image and ground truth image for each camera view, where the reconstruction loss is a combination of \mathcal{L}_1 loss and structural similarity index measure (SSIM) loss \mathcal{L}_{D-SSIM} :

$$\min_{\mathcal{G}} \mathcal{L}(\mathcal{D}) = \min_{\mathcal{G}} \sum_{k=1}^N \mathcal{L}(V'_k, V_k) = \min_{\mathcal{G}} \sum_{k=1}^N (1 - \lambda) \mathcal{L}_1(V'_k, V_k) + \lambda \mathcal{L}_{D-SSIM}(V'_k, V_k), \quad (6)$$

where λ is a trade-off parameter. To ensure finer reconstruction, Gaussian Splatting deploys *adaptive density control* to automatically add or remove Gaussians from optimization. The process of adding Gaussians, known as densification, involves two primary operations: splitting and cloning. Conversely, removing Gaussians, called pruning, indicates eliminating a Gaussian from the set of optimization variables. Both densification and pruning are non-differentiable operations. The adaptive density control is performed during regular optimization intervals and follows specific, predefined rules. In the

initial design (Kerbl et al., 2023), for a Gaussian G_i with view-space projection point $\mu_i^k = (\mu_{i,x}^k, \mu_{i,y}^k)$ under viewpoint V_k , the average view-space positional gradient $\nabla_{\mu_i} \mathcal{L}$ is calculated every 100 training iterations (Ye et al., 2024):

$$\nabla_{\mu_i} \mathcal{L} = \frac{\sum_{k=1}^M \left\| \frac{\partial \mathcal{L}(V'_k, V_k)}{\partial \mu_i^k} \right\|}{M}, \quad (7)$$

where M is the total number of views that the Gaussian G_i participates in calculation during the 100 iterations (Ye et al., 2024) and M is usually less than N . Densification is performed when the view-space positional gradient $\nabla_{\mu_i} \mathcal{L}$ is larger than a pre-set gradient threshold τ_g (by default 0.0002). Moreover, the decision to split or clone a Gaussian G_i is based on its scale vector s_i , which is compared with a scale threshold τ_s : it is split if larger, and cloned if smaller. Pruning occurs when the opacity α_i falls below the opacity threshold τ_α . We also notice some recent 3DGS studies (Cheng et al., 2024; Fang & Wang, 2024; Li et al., 2024; Bulò et al., 2024) that adopt different yet still pre-defined densification rules.

C THREAT MODEL

We provide a structured description of the attack’s goal, input, output, information and constraints in this section, to provide more clarity of the threat model:

Attacker Goal: To increase the computation cost and over-consume computation resource of 3DGS service provider.

Attacker Input: Clean data.

Attacker Output: Poisoned data by running attack on the clean data.

Attacker Information: Attacker doesn’t need to know the underlying hardware device of the victim.

- White-box: Attacker knows the specific 3DGS configuration of the victim.
- Black-box: Attacker only knows victim is using 3DGS, but does not know which variant of 3DGS representation and what configuration the victim is using.

Attacker Constraint: Attacker can optionally choose to constrain the perturbation range ϵ of his additive perturbation to add on clean data.

Attacker Algorithm: Algorithm 1.

Table 3: Full constrained attack results ($\epsilon = 16/255$) on all scenes from the NeRF-Synthetic, MIP-NeRF360 and Tanks-and-Temples datasets. All results are reported by averaging over three individual runs.

Constrained Poison-splat attack with $\epsilon = 16/255$									
Metric	Number of Gaussians		Peak GPU memory [MB]		Training time [minutes]		Render speed [FPS]		
Scene	Setting	clean	poisoned	clean	poisoned	clean	poisoned	clean	poisoned
NS-chair		0.494 M	0.957 M (1.94x \uparrow)	3752	8003 (2.13x \uparrow)	9.45	13.41 (1.42x \uparrow)	260	117 (2.22x \downarrow)
NS-drums		0.385 M	0.695 M (1.81x \uparrow)	3456	7190 (2.08x \uparrow)	8.75	11.94 (1.36x \uparrow)	347	144 (2.41x \downarrow)
NS-ficus		0.265 M	0.273 M (1.03x \uparrow)	3194	3783 (1.18x \uparrow)	6.99	8.94 (1.28x \uparrow)	346	337 (1.03x \downarrow)
NS-hotdog		0.185 M	1.147 M (6.20x \uparrow)	3336	29747* (8.92x \uparrow)	8.57	17.43 (2.03x \uparrow)	443	69 (6.42x \downarrow)
NS-lego		0.341 M	0.805 M (2.36x \uparrow)	3532	9960 (2.82x \uparrow)	8.62	13.02 (1.51x \uparrow)	349	145 (2.41x \downarrow)
NS-materials		0.169 M	0.410 M (2.43x \uparrow)	3172	4886 (1.54x \uparrow)	7.33	9.92 (1.35x \uparrow)	447	250 (1.79x \downarrow)
NS-mic		0.205 M	0.359 M (1.75x \uparrow)	3499	6437 (1.84x \uparrow)	8.08	10.96 (1.36x \uparrow)	300	172 (1.74x \downarrow)
NS-ship		0.272 M	1.071 M (3.94x \uparrow)	3692	16666 (4.51x \uparrow)	8.87	16.12 (1.82x \uparrow)	326	87 (3.75x \downarrow)
MIP-bicycle		5.793 M	10.129 M (1.75x \uparrow)	17748	27074* (1.53x \uparrow)	33.42	44.44 (1.33x \uparrow)	69	43 (1.60x \downarrow)
MIP-bonsai		1.294 M	6.150 M (4.75x \uparrow)	10216	20564 (2.01x \uparrow)	21.68	32.51 (1.50x \uparrow)	214	66 (3.24x \downarrow)
MIP-counter		1.195 M	4.628 M (3.87x \uparrow)	10750	29796* (2.77x \uparrow)	26.46	37.63 (1.42x \uparrow)	164	51 (3.22x \downarrow)
MIP-flowers		3.508 M	5.177 M (1.48x \uparrow)	12520	16338 (1.30x \uparrow)	25.47	30.05 (1.18x \uparrow)	124	89 (1.39x \downarrow)
MIP-garden		5.684 M	7.697 M (1.35x \uparrow)	17561	23115 (1.32x \uparrow)	33.19	40.82 (1.23x \uparrow)	81	54 (1.50x \downarrow)
MIP-kitchen		1.799 M	6.346 M (3.53x \uparrow)	12442	20902 (1.68x \uparrow)	26.61	43.24 (1.62x \uparrow)	133	46 (2.89x \downarrow)
MIP-room		1.513 M	7.129 M (4.71x \uparrow)	12316	46238* (3.75x \uparrow)	25.36	47.98 (1.89x \uparrow)	154	35 (4.40x \downarrow)
MIP-stump		4.671 M	10.003 M (2.14x \uparrow)	14135	25714* (1.82x \uparrow)	27.06	38.48 (1.42x \uparrow)	111	57 (1.95x \downarrow)
MIP-treehill		3.398 M	5.684 M (1.67x \uparrow)	11444	17287 (1.51x \uparrow)	22.76	29.26 (1.29x \uparrow)	123	70 (1.76x \downarrow)
TT-Auditorium		0.699 M	2.719 M (3.89x \uparrow)	5982	14532 (2.43x \uparrow)	12.69	19.05 (1.50x \uparrow)	266	100 (2.66x \downarrow)
TT-Ballroom		3.103 M	3.957 M (1.28x \uparrow)	10416	12226 (1.17x \uparrow)	20.37	22.43 (1.10x \uparrow)	96	85 (1.13x \downarrow)
TT-Barn		1.005 M	1.865 M (1.86x \uparrow)	7813	10470 (1.34x \uparrow)	13.10	16.27 (1.24x \uparrow)	229	127 (1.80x \downarrow)
TT-Caterpillar		1.290 M	1.857 M (1.44x \uparrow)	6624	8014 (1.21x \uparrow)	11.96	14.77 (1.23x \uparrow)	228	164 (1.39x \downarrow)
TT-Church		2.351 M	3.396 M (1.44x \uparrow)	10076	11797 (1.17x \uparrow)	17.43	20.54 (1.18x \uparrow)	132	97 (1.36x \downarrow)
TT-Courthouse		0.604 M	0.733 M (1.21x \uparrow)	11402	12688 (1.11x \uparrow)	13.81	14.49 (1.05x \uparrow)	284	220 (1.29x \downarrow)
TT-Courtroom		2.890 M	5.450 M (1.89x \uparrow)	9896	16308 (1.65x \uparrow)	16.88	23.92 (1.42x \uparrow)	139	83 (1.67x \downarrow)
TT-Family		2.145 M	3.734 M (1.74x \uparrow)	7261	10707 (1.47x \uparrow)	13.58	18.46 (1.36x \uparrow)	182	111 (1.64x \downarrow)
TT-Francis		0.759 M	1.612 M (2.12x \uparrow)	5208	6938 (1.33x \uparrow)	10.19	13.92 (1.37x \uparrow)	279	168 (1.66x \downarrow)
TT-Horse		1.308 M	2.510 M (1.92x \uparrow)	5125	7762 (1.51x \uparrow)	12.05	16.47 (1.37x \uparrow)	220	121 (1.82x \downarrow)
TT-Ignatius		3.144 M	3.937 M (1.25x \uparrow)	9943	11800 (1.19x \uparrow)	16.32	18.52 (1.13x \uparrow)	149	118 (1.26x \downarrow)
TT-Lighthouse		0.888 M	1.178 M (1.33x \uparrow)	7466	8696 (1.16x \uparrow)	14.21	15.92 (1.12x \uparrow)	213	163 (1.31x \downarrow)
TT-M60		1.667 M	2.980 M (1.79x \uparrow)	7948	10874 (1.37x \uparrow)	14.08	18.22 (1.29x \uparrow)	200	107 (1.87x \downarrow)
TT-Meetingroom		1.267 M	2.927 M (2.31x \uparrow)	6645	10234 (1.54x \uparrow)	13.53	18.97 (1.40x \uparrow)	197	102 (1.93x \downarrow)
TT-Museum		4.439 M	7.130 M (1.61x \uparrow)	12704	18790 (1.48x \uparrow)	19.79	26.38 (1.33x \uparrow)	121	78 (1.55x \downarrow)
TT-Palace		0.711 M	0.696 M (0.98x \uparrow)	8980	8372 (0.93x \uparrow)	14.27	14.54 (1.02x \uparrow)	185	186 (0.99x \downarrow)
TT-Panther		1.812 M	3.457 M (1.91x \uparrow)	8511	12048 (1.42x \uparrow)	13.49	19.46 (1.44x \uparrow)	199	103 (1.93x \downarrow)
TT-Playground		2.309 M	4.307 M (1.87x \uparrow)	8717	13032 (1.50x \uparrow)	15.17	21.82 (1.44x \uparrow)	151	87 (1.74x \downarrow)
TT-Temple		0.893 M	1.345 M (1.51x \uparrow)	6929	7525 (1.09x \uparrow)	13.03	15.26 (1.17x \uparrow)	216	149 (1.45x \downarrow)
TT-Train		1.113 M	1.332 M (1.20x \uparrow)	6551	7128 (1.09x \uparrow)	12.64	13.62 (1.08x \uparrow)	193	163 (1.18x \downarrow)
TT-Truck		2.533 M	3.630 M (1.43x \uparrow)	8662	11014 (1.27x \uparrow)	14.64	20.12 (1.37x \uparrow)	156	88 (1.77x \downarrow)

D EXTENDED EXPERIMENTS

D.1 FULL ATTACK RESULTS

We report the constrained attack results with $\epsilon = 16/255$ on all scenes of NeRF-Synthetic, Mip-NeRF360 and Tanks-and-Temples dataset in Table 3, and the unconstrained attack results in Table 4.

Table 4: Full unconstrained attack results ($\epsilon = \infty$) on all scenes from the NeRF-Synthetic, MIP-NeRF360 and Tanks-and-Temples datasets. All results are reported by averaging over three individual runs.

Unconstrained Poison-splat attack with $\epsilon = \infty$									
Metric	Number of Gaussians		Peak GPU memory [MB]		Training time [minutes]		Render speed [FPS]		
Scene	Setting	clean	poisoned	clean	poisoned	clean	poisoned	clean	poisoned
NS-chair		0.494 M	4.152 M (8.40x↑)	3752	51424* (13.71x↑)	9.45	40.71 (4.31x↑)	260	27 (9.63x↓)
NS-drums		0.385 M	4.109 M (10.67x↑)	3456	62328* (18.03x↑)	8.75	43.25 (4.94x↑)	347	24 (14.46x↓)
NS-ficus		0.265 M	3.718 M (14.03x↑)	3194	50450* (15.80x↑)	6.99	36.92 (5.28x↑)	346	31 (11.16x↓)
NS-hotdog		0.185 M	4.272 M (23.09x↑)	3336	47859* (14.35x↑)	8.57	38.85 (4.53x↑)	443	29 (15.28x↓)
NS-lego		0.341 M	4.159 M (12.20x↑)	3532	78852* (22.33x↑)	8.62	42.46 (4.93x↑)	349	25 (13.96x↓)
NS-materials		0.169 M	3.380 M (20.00x↑)	3172	43998* (13.87x↑)	7.33	32.40 (4.42x↑)	447	37 (12.08x↓)
NS-mic		0.205 M	3.940 M (19.22x↑)	3499	61835* (17.67x↑)	8.08	39.02 (4.83x↑)	300	29 (10.34x↓)
NS-ship		0.272 M	4.317 M (15.87x↑)	3692	80956* (21.93x↑)	8.87	44.11 (4.97x↑)	326	24 (13.58x↓)
MIP-bicycle		5.793 M	25.268 M (4.36x↑)	17748	63236* (3.56x↑)	33.42	81.48 (2.44x↑)	69	16 (4.31x↓)
MIP-bonsai		1.294 M	20.127 M (15.55x↑)	10216	54506* (5.34x↑)	21.68	75.18 (3.47x↑)	214	18 (11.89x↓)
MIP-counter		1.195 M	11.167 M (9.34x↑)	10750	80732* (7.51x↑)	26.46	62.04 (2.34x↑)	164	19 (8.63x↓)
MIP-flowers		3.508 M	18.075 M (5.15x↑)	12520	45515* (3.64x↑)	25.47	62.62 (2.46x↑)	124	24 (5.17x↓)
MIP-garden		5.684 M	21.527 M (3.79x↑)	17561	52140* (2.97x↑)	33.19	83.81 (2.53x↑)	81	17 (4.76x↓)
MIP-kitchen		1.799 M	12.830 M (7.13x↑)	12442	77141* (6.20x↑)	26.61	73.04 (2.74x↑)	133	16 (8.31x↓)
MIP-room		1.513 M	16.019 M (10.59x↑)	12316	57540* (4.67x↑)	25.36	76.25 (3.01x↑)	154	17 (9.06x↓)
MIP-stump		4.671 M	13.550 M (2.90x↑)	14135	36181* (2.56x↑)	27.06	51.51 (1.90x↑)	111	27 (4.11x↓)
MIP-treehill		3.398 M	13.634 M (4.01x↑)	11444	36299* (3.17x↑)	22.76	52.83 (2.32x↑)	123	24 (5.12x↓)
TT-Auditorium		0.699 M	4.153 M (5.94x↑)	5982	12666 (2.12x↑)	12.69	22.50 (1.77x↑)	266	76 (3.50x↓)
TT-Ballroom		3.103 M	7.534 M (2.43x↑)	10416	19832 (1.90x↑)	20.37	33.63 (1.65x↑)	96	46 (2.09x↓)
TT-Barn		1.005 M	5.456 M (5.43x↑)	7813	15682 (2.01x↑)	13.10	26.10 (1.99x↑)	229	61 (3.75x↓)
TT-Caterpillar		1.290 M	6.980 M (5.41x↑)	6624	18909 (2.85x↑)	11.96	29.51 (2.47x↑)	228	53 (4.30x↓)
TT-Church		2.351 M	7.564 M (3.22x↑)	10076	21296 (2.11x↑)	17.43	33.39 (1.92x↑)	132	43 (3.07x↓)
TT-Courthouse		0.604 M	3.388 M (5.61x↑)	11402	29856* (2.62x↑)	13.81	25.33 (1.83x↑)	284	54 (5.26x↓)
TT-Courtroom		2.890 M	13.196 M (4.57x↑)	9896	33871* (3.42x↑)	16.88	41.69 (2.47x↑)	139	41 (3.39x↓)
TT-Family		2.145 M	11.700 M (5.45x↑)	7261	27533* (3.79x↑)	13.58	38.79 (2.86x↑)	182	43 (4.23x↓)
TT-Francis		0.759 M	7.435 M (9.80x↑)	5208	19777 (3.80x↑)	10.19	31.01 (3.04x↑)	279	51 (5.47x↓)
TT-Horse		1.308 M	9.358 M (7.15x↑)	5125	22756 (4.44x↑)	12.05	34.90 (2.90x↑)	220	46 (4.78x↓)
TT-Ignatius		3.144 M	11.278 M (3.59x↑)	9943	28895* (2.91x↑)	16.32	39.61 (2.43x↑)	149	42 (3.55x↓)
TT-Lighthouse		0.888 M	5.081 M (5.72x↑)	7466	23842 (3.19x↑)	14.21	30.67 (2.16x↑)	213	47 (4.53x↓)
TT-M60		1.667 M	7.076 M (4.24x↑)	7948	21062 (2.65x↑)	14.08	31.82 (2.26x↑)	200	46 (4.35x↓)
TT-Meetingroom		1.267 M	7.066 M (5.58x↑)	6645	19182 (2.89x↑)	13.53	31.44 (2.32x↑)	197	50 (3.94x↓)
TT-Museum		4.439 M	16.501 M (3.72x↑)	12704	43317* (3.41x↑)	19.79	48.89 (2.47x↑)	121	36 (3.36x↓)
TT-Palace		0.711 M	2.764 M (3.89x↑)	8980	14065 (1.57x↑)	14.27	20.07 (1.41x↑)	185	84 (2.20x↓)
TT-Panther		1.812 M	8.112 M (4.48x↑)	8511	22638 (2.66x↑)	13.49	33.19 (2.46x↑)	199	49 (4.06x↓)
TT-Playground		2.309 M	10.306 M (4.46x↑)	8717	27304* (3.13x↑)	15.17	38.77 (2.56x↑)	151	39 (3.87x↓)
TT-Temple		0.893 M	5.231 M (5.86x↑)	6929	15238 (2.20x↑)	13.03	27.96 (2.15x↑)	216	52 (4.15x↓)
TT-Train		1.113 M	4.916 M (4.42x↑)	6551	14840 (2.27x↑)	12.64	25.34 (2.00x↑)	193	59 (3.27x↓)
TT-Truck		2.533 M	8.004 M (3.16x↑)	8662	21166 (2.44x↑)	14.64	33.26 (2.27x↑)	156	47 (3.32x↓)

D.2 FULL BLACK-BOX ATTACK RESULTS

We report the full results of attacking a black-box victim (Scaffold-GS) (Lu et al., 2024) on NeRF-Synthetic and MIP-NeRF360 datasets in Table 5.

To further test the effectiveness of Poison-Splat, we conduct black-box attack experiments on Mip-Splatting (Yu et al., 2024), which received the best student paper award at CVPR 2024 and has been highly popular (with 178 citations as of November 20th, 2024). Mip-Splatting is an advanced variant of the original 3D Gaussian Splatting, incorporating a 3D smoothing filter and a 2D Mip filter. These enhancements help eliminate various artifacts and achieve alias-free renderings. Results are shown in Table 6.

We found that Mip-Splatting (Yu et al., 2024) consumes more GPU memory compared to the original 3D Gaussian Splatting, making it more prone to the worst attack consequence of running Out-of-Memory. As illustrated in Table 6, even when the attack perturbation is constrained to $\epsilon = 16/255$, the GPU memory consumption nearly reached the 80 GB capacity of Nvidia A800. When we apply an unconstrained attack, all scenes in the MIP-NeRF360 dataset will result in denial-of-service.

Table 5: Full black-box attack results on NeRF-Synthetic and MIP-NeRF360 datasets. The victim system, Scaffold-GS, utilizes distinctly different Gaussian Splatting feature representations compared to traditional Gaussian Splatting and remains unknown to the attacker. These results demonstrate the robust generalization ability of our attack against unknown black-box victim systems.

Constrained Black-box Poison-splat attack with $\epsilon = 16/255$ against Scaffold-GS						
Metric	Number of Gaussians		Peak GPU memory [MB]		Training time [minutes]	
Setting \ Scene	clean	poisoned	clean	poisoned	clean	poisoned
NS-chair	1.000 M	1.615 M (1.61x \uparrow)	3418	4003 (1.17x \uparrow)	9.91	17.18 (1.73x \uparrow)
NS-drums	1.000 M	1.771 M (1.77x \uparrow)	4022	4382 (1.09x \uparrow)	10.62	16.29 (1.53x \uparrow)
NS-ficus	1.000 M	2.301 M (2.30x \uparrow)	3416	4234 (1.24x \uparrow)	9.64	18.54 (1.92x \uparrow)
NS-hotdog	1.000 M	1.463 M (1.46x \uparrow)	3539	4516 (1.28x \uparrow)	10.74	18.62 (1.73x \uparrow)
NS-lego	0.414 M	2.074 M (5.01x \uparrow)	3003	4808 (1.60x \uparrow)	9.77	17.91 (1.83x \uparrow)
NS-materials	1.000 M	2.520 M (2.52x \uparrow)	4110	5190 (1.26x \uparrow)	10.87	17.75 (1.63x \uparrow)
NS-mic	1.000 M	2.053 M (2.05x \uparrow)	3682	5054 (1.37x \uparrow)	10.36	18.53 (1.79x \uparrow)
NS-ship	1.000 M	3.291 M (3.29x \uparrow)	3492	5024 (1.44x \uparrow)	11.68	21.92 (1.88x \uparrow)
MIP-bicycle	8.883 M	16.947 M (1.91x \uparrow)	12817	13650 (1.06x \uparrow)	38.93	44.98 (1.16x \uparrow)
MIP-bonsai	4.368 M	10.608 M (2.43x \uparrow)	10080	12218 (1.21x \uparrow)	35.33	37.71 (1.07x \uparrow)
MIP-counter	2.910 M	6.387 M (2.19x \uparrow)	12580	17702 (1.41x \uparrow)	38.53	44.83 (1.16x \uparrow)
MIP-flowers	7.104 M	11.614 M (1.63x \uparrow)	8241	9766 (1.19x \uparrow)	36.56	38.31 (1.05x \uparrow)
MIP-garden	7.630 M	11.555 M (1.51x \uparrow)	9194	10966 (1.19x \uparrow)	38.57	42.79 (1.11x \uparrow)
MIP-kitchen	3.390 M	6.698 M (1.98x \uparrow)	14037	16895 (1.20x \uparrow)	43.83	48.10 (1.10x \uparrow)
MIP-room	2.846 M	10.527 M (3.70x \uparrow)	13323	13981 (1.05x \uparrow)	36.24	48.01 (1.32x \uparrow)
MIP-stump	6.798 M	14.544 M (2.14x \uparrow)	7322	9432 (1.29x \uparrow)	33.53	36.32 (1.08x \uparrow)
Unconstrained Black-box Poison-splat attack with $\epsilon = \infty$ against Scaffold-GS						
Metric	Number of Gaussians		Peak GPU memory [MB]		Training time [minutes]	
Setting \ Scene	clean	poisoned	clean	poisoned	clean	poisoned
NS-chair	1.000 M	3.082 M (3.08x \uparrow)	3418	5197 (1.52x \uparrow)	9.91	25.34 (2.56x \uparrow)
NS-drums	1.000 M	5.026 M (5.03x \uparrow)	4022	7364 (1.83x \uparrow)	10.62	28.24 (2.66x \uparrow)
NS-ficus	1.000 M	2.106 M (2.11x \uparrow)	3416	4446 (1.30x \uparrow)	9.64	21.65 (2.25x \uparrow)
NS-hotdog	1.000 M	3.541 M (3.54x \uparrow)	3539	5492 (1.55x \uparrow)	10.74	24.93 (2.32x \uparrow)
NS-lego	0.414 M	3.973 M (9.60x \uparrow)	3003	6242 (2.08x \uparrow)	9.77	26.11 (2.67x \uparrow)
NS-materials	1.000 M	3.997 M (4.00x \uparrow)	4110	5997 (1.46x \uparrow)	10.87	25.48 (2.34x \uparrow)
NS-mic	1.000 M	3.021 M (3.02x \uparrow)	3682	5490 (1.49x \uparrow)	10.36	23.71 (2.29x \uparrow)
NS-ship	1.000 M	4.717 M (4.72x \uparrow)	3492	6802 (1.95x \uparrow)	11.68	28.22 (2.42x \uparrow)
MIP-bicycle	8.883 M	33.284 M (3.75x \uparrow)	12817	22042 (1.72x \uparrow)	38.93	84.71 (2.18x \uparrow)
MIP-bonsai	4.368 M	28.042 M (6.42x \uparrow)	10080	22115 (2.19x \uparrow)	35.33	78.36 (2.22x \uparrow)
MIP-counter	2.910 M	12.928 M (4.44x \uparrow)	12580	16168 (1.29x \uparrow)	38.53	55.59 (1.44x \uparrow)
MIP-flowers	7.104 M	27.610 M (3.89x \uparrow)	8241	18352 (2.23x \uparrow)	36.56	73.43 (2.01x \uparrow)
MIP-garden	7.630 M	23.828 M (3.12x \uparrow)	9194	20400 (2.22x \uparrow)	38.57	85.45 (2.22x \uparrow)
MIP-kitchen	3.390 M	14.404 M (4.25x \uparrow)	14037	17838 (1.27x \uparrow)	43.83	63.32 (1.44x \uparrow)
MIP-room	2.846 M	21.060 M (7.40x \uparrow)	13323	21672 (1.63x \uparrow)	36.24	76.94 (2.12x \uparrow)
MIP-stump	6.798 M	34.027 M (5.01x \uparrow)	7322	20797 (2.84x \uparrow)	33.53	79.64 (2.38x \uparrow)

We examined the code implementation of Mip-Splatting⁶, and identified that it uses quantile computation in its Gaussian model densification function⁷ which requires massive GPU memory and easily triggers out-of-memory. Our attack highlights the vulnerability in various 3DGS algorithm implementations.

⁶<https://github.com/autonomousvision/mip-splatting>

⁷In Line 524 of `mip-splatting/scene/gaussian_model.py`

Table 6: Black-box attack results on Mip-Splatting (Yu et al., 2024) as the victim system, which can further demonstrate the robust generalization ability of our attack against unknown black-box victim systems.

Constrained Black-box Poison-splat attack with $\epsilon = 16/255$ against Mip-Splatting						
Metric	Number of Gaussians		Peak GPU memory [MB]		Training time [minutes]	
Setting	clean	poisoned	clean	poisoned	clean	poisoned
Scene						
NS-chair	0.372 M	1.088 M (2.92x \uparrow)	6318	33042* (5.23x \uparrow)	7.85	13.75 (1.75x \uparrow)
NS-drums	0.429 M	0.773 M (1.80x \uparrow)	7474	22036 (2.95x \uparrow)	8.15	12.60 (1.55x \uparrow)
NS-ficus	0.234 M	0.420 M (1.79x \uparrow)	6144	12374 (2.01x \uparrow)	6.35	8.97 (1.41x \uparrow)
NS-hotdog	0.200 M	1.437 M (7.18x \uparrow)	5350	58878* (11.01x \uparrow)	7.08	20.08 (2.84x \uparrow)
NS-lego	0.307 M	1.127 M (3.67x \uparrow)	6696	48682* (7.27x \uparrow)	7.28	16.43 (2.26x \uparrow)
NS-materials	0.216 M	0.505 M (2.34x \uparrow)	5278	9674 (1.83x \uparrow)	6.72	8.88 (1.32x \uparrow)
NS-mic	0.268 M	0.557 M (2.08x \uparrow)	5338	19758 (3.70x \uparrow)	9.12	12.23 (1.34x \uparrow)
NS-ship	0.330 M	1.793 M (5.43x \uparrow)	6500	61026* (9.39x \uparrow)	8.75	21.05 (2.41x \uparrow)
MIP-bicycle	8.683 M	DoS	80614	DoS	47.57	DoS
MIP-bonsai	1.670 M	13.016 M (7.79x \uparrow)	30876	80826* (2.62x \uparrow)	23.72	61.82 (2.61x \uparrow)
MIP-counter	1.493 M	8.329 M (5.58x \uparrow)	19478	79904* (4.10x \uparrow)	26.25	56.75 (2.16x \uparrow)
MIP-flowers	3.834 M	7.281 M (1.90x \uparrow)	50922	80286* (1.58x \uparrow)	32.85	41.80 (1.27x \uparrow)
MIP-garden	5.828 M	8.677 M (1.49x \uparrow)	70446	80440* (1.14x \uparrow)	43.20	54.43 (1.26x \uparrow)
MIP-kitchen	2.182 M	10.734 M (4.92x \uparrow)	37024	81006* (2.19x \uparrow)	30.63	66.92 (2.18x \uparrow)
MIP-room	2.080 M	12.949 M (6.23x \uparrow)	31616	81130* (2.57x \uparrow)	27.13	77.83 (2.87x \uparrow)
MIP-stump	5.920 M	13.925 M (2.35x \uparrow)	65882	80480* (1.22x \uparrow)	34.33	56.43 (1.64x \uparrow)
Unconstrained Black-box Poison-splat attack with $\epsilon = \infty$ against Mip-Splatting						
Metric	Number of Gaussians		Peak GPU memory [MB]		Training time [minutes]	
Setting	clean	poisoned	clean	poisoned	clean	poisoned
Scene						
NS-chair	0.372 M	6.106 M (16.41x \uparrow)	6318	80732* (12.78x \uparrow)	7.85	57.73 (7.35x \uparrow)
NS-drums	0.429 M	6.818 M (15.89x \uparrow)	7474	81210* (10.87x \uparrow)	8.15	67.67 (8.30x \uparrow)
NS-ficus	0.234 M	4.847 M (20.71x \uparrow)	6144	80834* (13.16x \uparrow)	6.35	45.85 (7.22x \uparrow)
NS-hotdog	0.200 M	6.876 M (34.38x \uparrow)	5350	80630* (15.07x \uparrow)	7.08	59.80 (8.45x \uparrow)
NS-lego	0.307 M	6.472 M (21.08x \uparrow)	6696	80668* (12.05x \uparrow)	7.28	64.93 (8.92x \uparrow)
NS-materials	0.216 M	5.513 M (25.52x \uparrow)	5278	81112* (15.37x \uparrow)	6.72	45.08 (6.71x \uparrow)
NS-mic	0.268 M	5.433 M (20.27x \uparrow)	5338	81020* (15.18x \uparrow)	9.12	52.83 (5.79x \uparrow)
NS-ship	0.330 M	6.848 M (20.75x \uparrow)	6500	81236* (12.50x \uparrow)	8.75	66.15 (7.56x \uparrow)
MIP-bicycle	8.683 M	DoS	80614	DoS	47.57	DoS
MIP-bonsai	1.670 M	DoS	30876	DoS	23.72	DoS
MIP-counter	1.493 M	DoS	19478	DoS	26.25	DoS
MIP-flowers	3.834 M	DoS	50922	DoS	32.85	DoS
MIP-garden	5.828 M	DoS	70446	DoS	43.20	DoS
MIP-kitchen	2.182 M	DoS	37024	DoS	30.63	DoS
MIP-room	2.080 M	DoS	31616	DoS	27.13	DoS
MIP-stump	5.920 M	DoS	65882	DoS	34.33	DoS

E NOTATIONS

We provide Table 7 to list all the notations appeared in the paper.

F VISUALIZATIONS

In this section, we present both the attacker-crafted poisoned images and the resultant reconstructions by the victim model. The visualizations aim to provide readers with more straightforward understanding of our attack. The constrained attack visualizations are provided in Table 8, and the unconstrained attack visualizations are provided in Table 9.

We have following interesting observations:

Table 7: Notation List

Variable	Description
\mathcal{G}	3D Gaussians
$\ \mathcal{G}\ $	The number of 3D Gaussians
G_i	The i -th Gaussian in the scene
\mathcal{D}	Clean image datasets
\mathcal{D}_p	Poisoned image datasets
V_k	The k -th camera view’s clean image
P_k	The k -th camera view’s camera pose
\tilde{V}_k	The k -th camera view’s poisoned image
\tilde{P}_k	The k -th camera view’s poisoned pose
V'_k	The k -th camera view’s rendered image
N	The total number of views
$\mu \in \mathbb{R}^3$	Center 3D coordinates (positions) of a Gaussian
$s \in \mathbb{R}^3$	3D scales of a Gaussian
$\alpha \in \mathbb{R}$	Opacity of a Gaussian
$q \in \mathbb{R}^4$	Rotation quaternion of a Gaussian
$c \in \mathbb{R}^{3 \times (d+1)^2}$	Color of a Gaussian represented as spherical harmonics, where d is the degree
τ_g	Gradient threshold
τ_s	Scale threshold
τ_α	Opacity threshold
\mathcal{R}	Renderer function
ϵ	Perturbation range
η	Perturbation step size
T	The iteration number of inner optimization
\tilde{T}	The iteration number of outer optimization
$\mathcal{P}_\epsilon(\cdot)$	Projection into ϵ -ball
\mathcal{L}	Reconstruction loss
\mathcal{L}_1	\mathcal{L}_1 loss
\mathcal{L}_{D-SSIM}	Structural similarity index measure (SSIM) loss
$\mathcal{C}(\mathcal{G}^*)$	Training costs of 3D Gaussians
$\mathcal{S}_{TV}(V_k)$	Total variation score
λ	Loss trade-off parameters

- Unconstrained Poisoned Attacks:** On both NeRF-Synthetic and MIP-NeRF360, the reconstruction results consistently show a low PSNR (around 20 dB). While the poisoned images and victim reconstructions may both resemble chaotic arrangements of lines with needle-like Gaussians, subtle differences in detail exist. These differences, though difficult for the human eye to distinguish, are reflected in the PSNR.
- Constrained Attacks on NeRF-Synthetic:** the reconstruction results are significantly better than unconstrained attacks, with an average PSNR of around 30 dB.
- Constrained Attacks on MIP-NeRF360:** There are substantial appearance differences between the victim reconstructions and the poisoned input images, which are easily noticeable through human observation. Specifically, in the bicycle scene, the reconstructed trees appear to have denser leaves. In the bonsai and counter scenes, we observe notable changes in reflective areas, with several reflection highlights disappearing in the victim’s reconstructed images. Additionally, in the counter scene, there is evidence of underfitting, where the complex textures of the poisoned data degrade into large, blurry floaters in the victim’s reconstruction.

Table 8: Attacker poisoned and victim reconstructed images with PSNR values under constrained attack ($\epsilon = 16/255$) settings.









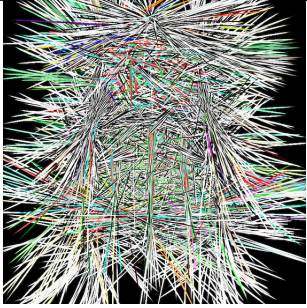
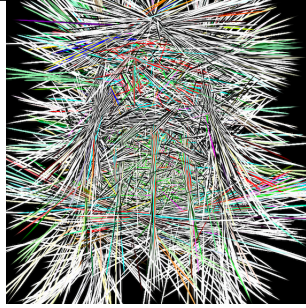
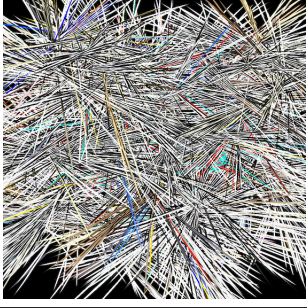
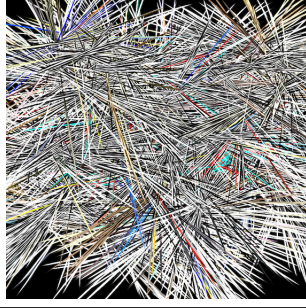
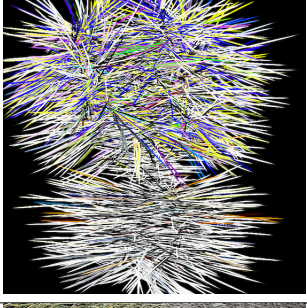
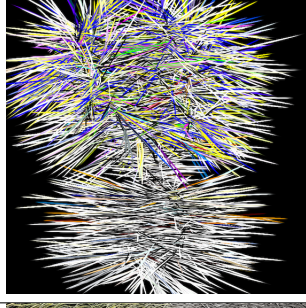






Dataset Setting	Attacker Poisoned Image	Victim Reconstructed Image	PSNR
NS-Chair			37.07 dB
NS-Drums			30.32 dB
NS-Ficus			35.77 dB
MIP-bicycle			18.20 dB
MIP-bonsai			22.67 dB
MIP-counter			24.45 dB

Table 9: Attacker poisoned and victim reconstructed images with PSNR values under unconstrained attack settings.

Dataset Scene	Attacker Poisoned Image	Victim Reconstructed Image	PSNR
NS-Chair			19.54 dB
NS-Drums			18.65 dB
NS-Ficus			21.00 dB
MIP-bicycle			20.57 dB
MIP-bonsai			23.66 dB
MIP-counter			21.33 dB

1350 Table 10: Attack performance (number of Gaussians, GPU memory consumption and training
 1351 time) and image quality (SSIM and PSNR compared with clean images) under different levels of
 1352 perturbation range on NeRF Synthetic dataset.

1354	Scene	Attack setting	Number of Gaussians	GPU memory	Training time	SSIM	PSNR
1355	chair	clean	0.494 M	3752 MB	9.45 min	-	-
1356		$\epsilon = 8/255$	0.670 M	4520 MB	11.24 min	0.42	34.20
1357		$\epsilon = 16/255$	0.957 M	8003 MB	13.41 min	0.21	27.94
1358		$\epsilon = 24/255$	1.253 M	16394 MB	15.89 min	0.16	24.35
1359		unconstrained	4.152 M	51424 MB	40.71 min	0.07	4.63
1360	drums	clean	0.385 M	3456 MB	8.75 min	-	-
1361		$\epsilon = 8/255$	0.469 M	4353 MB	10.19 min	0.45	34.05
1362		$\epsilon = 16/255$	0.695 M	7190 MB	11.94 min	0.24	27.87
1363		$\epsilon = 24/255$	0.966 M	14668 MB	14.86 min	0.17	24.36
1364		unconstrained	4.109 M	62328 MB	43.25 min	0.03	4.49
1365	figus	clean	0.265 M	3194 MB	6.99 min	-	-
1366		$\epsilon = 8/255$	0.246 M	3238 MB	8.28 min	0.39	34.45
1367		$\epsilon = 16/255$	0.273 M	3783 MB	8.94 min	0.18	28.21
1368		$\epsilon = 24/255$	0.450 M	8993 MB	11.32 min	0.13	24.53
1369		unconstrained	3.718 M	50450 MB	36.92 min	0.08	4.41
1370	hotdog	clean	0.185 M	3336 MB	8.57 min	-	-
1371		$\epsilon = 8/255$	0.610 M	10362 MB	12.96 min	0.46	33.93
1372		$\epsilon = 16/255$	1.147 M	29747 MB	17.43 min	0.25	27.56
1373		$\epsilon = 24/255$	1.553 M	39087 MB	21.26 min	0.17	24.11
1374		unconstrained	4.272 M	47859 MB	38.85 min	0.07	5.75
1375	lego	clean	0.341 M	3532 MB	8.62 min	-	-
1376		$\epsilon = 8/255$	0.469 M	4648 MB	10.38 min	0.48	34.08
1377		$\epsilon = 16/255$	0.805 M	9960 MB	13.02 min	0.28	27.88
1378		$\epsilon = 24/255$	1.116 M	18643 MB	15.33 min	0.21	24.30
1379		unconstrained	4.159 M	78852 MB	42.46 min	0.06	4.78
1380	materials	clean	0.169 M	3172 MB	7.33 min	-	-
1381		$\epsilon = 8/255$	0.229 M	3581 MB	8.84 min	0.44	34.25
1382		$\epsilon = 16/255$	0.410 M	4886 MB	9.92 min	0.21	27.97
1383		$\epsilon = 24/255$	0.589 M	7724 MB	11.51 min	0.14	24.35
1384		unconstrained	3.380 M	43998 MB	32.40 min	0.08	5.40
1385	mic	clean	0.205 M	3499 MB	8.08 min	-	-
1386		$\epsilon = 8/255$	0.251 M	4038 MB	9.29 min	0.36	34.46
1387		$\epsilon = 16/255$	0.359 M	6437 MB	10.96 min	0.15	28.17
1388		$\epsilon = 24/255$	0.514 M	13014 MB	12.89 min	0.10	24.48
1389		unconstrained	3.940 M	61835 MB	39.02 min	0.08	4.50
1390	ship	clean	0.272 M	3692 MB	8.87 min	-	-
1391		$\epsilon = 8/255$	0.516 M	5574 MB	11.01 min	0.55	33.42
1392		$\epsilon = 16/255$	1.071 M	16666 MB	16.12 min	0.33	27.50
1393		$\epsilon = 24/255$	1.365 M	29828 MB	18.46 min	0.24	24.03
1394		unconstrained	4.317 M	80956 MB	44.11 min	0.04	5.31

1394 G ABLATION STUDY ON PERTURBATION RANGE

1395
 1396 We compare the attack effects (in terms of number of Gaussians, GPU memory and training time)
 1397 and image degradation (in terms of SSIM and PSNR compared with clean input) under different
 1398 perturbation ranges $\epsilon = 8$, $\epsilon = 16$, $\epsilon = 24$) on NeRF-Synthetic and MIP-NeRF360 datasets, as shown
 1399 in Table 10 and Table 11.

1400
 1401
 1402
 1403

Table 11: Attack performance (number of Gaussians, GPU memory consumption and training time) and image quality (SSIM and PSNR compared with clean images) under different levels of constraints on MIP-NeRF360 dataset.

Scene	Attack setting	Number of Gaussians	GPU memory (MB)	Training time (min)	SSIM	PSNR
bicycle	clean	5.793 M	17748	33.42	-	-
	$\epsilon = 8/255$	6.116 M	18608	34.73	0.86	30.80
	$\epsilon = 16/255$	10.129 M	27074	44.44	0.67	26.24
	$\epsilon = 24/255$	13.265 M	34870	51.37	0.52	23.12
	unconstrained	25.268 M	63236	81.48	0.02	6.60
bonsai	clean	1.294 M	10216	21.68	-	-
	$\epsilon = 8/255$	1.778 M	11495	21.39	0.79	32.45
	$\epsilon = 16/255$	6.150 M	20564	32.51	0.51	26.83
	$\epsilon = 24/255$	9.321 M	27191	39.84	0.35	23.52
	unconstrained	20.127 M	54506	75.18	0.01	6.27
counter	clean	1.195 M	10750	26.46	-	-
	$\epsilon = 8/255$	1.739 M	15133	28.06	0.80	32.24
	$\epsilon = 16/255$	4.628 M	29796	37.63	0.52	26.78
	$\epsilon = 24/255$	6.649 M	47607	43.68	0.35	23.45
	unconstrained	11.167 M	80732	62.04	0.01	6.64
flowers	clean	3.508 M	12520	25.47	-	-
	$\epsilon = 8/255$	3.457 M	12391	25.53	0.87	29.18
	$\epsilon = 16/255$	5.177 M	16338	30.05	0.71	25.60
	$\epsilon = 24/255$	7.280 M	20264	34.25	0.58	22.79
	unconstrained	18.075 M	45515	62.62	0.02	6.79
garden	clean	5.684 M	17561	33.19	-	-
	$\epsilon = 8/255$	5.122 M	16498	32.17	0.84	29.85
	$\epsilon = 16/255$	7.697 M	23115	40.82	0.68	25.87
	$\epsilon = 24/255$	10.356 M	28130	48.88	0.54	22.82
	unconstrained	21.527 M	52140	83.81	0.04	7.43
kitchen	clean	1.799 M	12442	26.61	-	-
	$\epsilon = 8/255$	2.675 M	13760	31.39	0.83	31.58
	$\epsilon = 16/255$	6.346 M	20902	43.24	0.60	26.52
	$\epsilon = 24/255$	9.445 M	27646	53.16	0.45	23.18
	unconstrained	12.830 M	77141	73.04	0.03	7.76
room	clean	1.513 M	12316	25.36	-	-
	$\epsilon = 8/255$	3.034 M	19542	32.99	0.75	32.41
	$\epsilon = 16/255$	7.129 M	46238	47.98	0.45	26.64
	$\epsilon = 24/255$	9.724 M	80142	56.87	0.29	23.32
	unconstrained	16.019 M	57540	76.25	0.01	6.42
stump	clean	4.671 M	14135	27.06	-	-
	$\epsilon = 8/255$	5.152 M	15342	28.21	0.84	31.20
	$\epsilon = 16/255$	10.003 M	25714	38.48	0.65	25.67
	$\epsilon = 24/255$	14.292 M	34246	46.89	0.49	22.98
	unconstrained	13.550 M	36181	51.51	0.02	7.14

H ABLATION STUDY ON POISON RATIO

In the main paper, we conducted all other experiments with 100% poison rate, based on the assumption that attacker can fully control data collection process. This assumption is reasonable for most 3D tasks, since the datasets typically are the same scene or object captured from different angles.

To gain deeper insights into the Poison-splat attack, we explore how varying levels of data poisoning ratio can affect the attack’s effectiveness. We conduct experiments using poison ratios of 20%, 40%, 60%, and 80%, and report the number of Gaussians, GPU memory consumption, and training time in Table 12. In these experiments, the poisoned views are randomly selected. To mitigate the effects of randomness, we report the mean value and standard deviation for each setting across three individual runs.

Table 12: Attack effectiveness under different poison ratio.

Scene	Poison Ratio	Number of Gaussians	GPU memory (MB)	Training time (min)
NS-hotdog-eps16	clean	0.185 M \pm 0.000 M	3336 MB \pm 11 MB	8.57 min \pm 0.30 min
	20%	0.203 M \pm 0.004 M	3286 MB \pm 70 MB	8.84 min \pm 0.27 min
	40%	0.279 M \pm 0.024 M	3896 MB \pm 286 MB	9.79 min \pm 0.53 min
	60%	0.501 M \pm 0.054 M	7367 MB \pm 1200 MB	11.33 min \pm 0.82 min
	80%	0.806 M \pm 0.018 M	13621 MB \pm 861 MB	14.02 min \pm 0.60 min
	100%	1.147 M \pm 0.003 M	29747 \pm 57 MB	17.43 min \pm 0.61 min
NS-ship-eps16	clean	0.272 M \pm 0.001 M	3692 MB \pm 52 MB	8.87 min \pm 0.44 min
	20%	0.321 M \pm 0.004 M	3764 MB \pm 70 MB	9.55 min \pm 0.17 min
	40%	0.472 M \pm 0.021 M	4796 MB \pm 293 MB	10.49 min \pm 0.58 min
	60%	0.718 M \pm 0.003 M	7034 MB \pm 407 MB	12.52 min \pm 0.45 min
	80%	0.924 M \pm 0.004 M	11850 MB \pm 510 MB	14.37 min \pm 0.60 min
	100%	1.071 M \pm 0.003 M	16666 MB \pm 548 MB	16.12 min \pm 0.42 min
MIP-counter-eps16	clean	1.195 M \pm 0.005 M	10750 MB \pm 104 MB	26.46 min \pm 0.57 min
	20%	1.221 M \pm 0.005 M	11043 MB \pm 141 MB	27.41 min \pm 0.85 min
	40%	1.358 M \pm 0.030 M	11535 MB \pm 147 MB	27.97 min \pm 0.47 min
	60%	2.005 M \pm 0.056 M	13167 MB \pm 227 MB	28.87 min \pm 0.52 min
	80%	3.273 M \pm 0.119 M	19578 MB \pm 1417 MB	32.99 min \pm 0.57 min
	100%	4.628 M \pm 0.014 M	29796 MB \pm 187 MB	37.63 min \pm 0.48 min
MIP-room-eps16	clean	1.513 M \pm 0.004 M	12316 MB \pm 13 MB	25.36 min \pm 0.09 min
	20%	1.520 M \pm 0.015 M	12624 MB \pm 502 MB	26.45 min \pm 0.75 min
	40%	1.938 M \pm 0.036 M	14495 MB \pm 320 MB	27.99 min \pm 0.72 min
	60%	3.589 M \pm 0.096 M	18760 MB \pm 765 MB	34.09 min \pm 0.79 min
	80%	5.503 M \pm 0.017 M	28166 MB \pm 457 MB	41.47 min \pm 1.36 min
	100%	7.129 M \pm 0.020 M	46238 MB \pm 802 MB	47.98 min \pm 0.72 min

From Table 12, we have following observations:

- Attack performance, in terms of both GPU memory usage and training time extension, becomes stronger as poisoning rate increases.
- At higher poisoning rates (between 60%-80%), the attack exhibits greater variance due to the randomness involved in selecting which views to poison. This suggests that the choice of views to poison can also impact the effectiveness of the attack.

I ABLATION STUDY ON DEFENSE THRESHOLD OF LIMITING GAUSSIAN NUMBERS

In the main paper, we set the defense threshold to ensure a tight wrapping of necessary Gaussians for reconstruction on the clean scene. More specifically, for three scenes we show in Section 4.4 and Figure 5, we set defense threshold as in the following Table 13:

For a 3DGS trainer, setting a uniform defense threshold is a notably challenging task due to the significant variance in different scenes. Implementing a low threshold can safeguard the victim’s computational resources from excessive consumption, but it may also substantially compromise

Table 13: Number of Gaussians on clean data and as defense threshold used in Section 4.4.

Scene	#Gaussians on clean data	#Gaussians as defense threshold
Bicycle	5.793 Million	6 Million
Flowers	3.508 Million	4 Million
Room	1.513 Million	2 Million

the quality of reconstruction for complex scenes. Choosing the defense threshold should consider this resource-quality tradeoff. Taking *room* of Nerf-Synthetic as an example, we tested the defense threshold across 2 million to 7 million, as shown in the following Table 14 and Figure 6:

Table 14: Defense threshold impact on GPU consumption and reconstruction PSNR.

Defense threshold	Max GPU memory (MB)	Reconstruction PSNR
<i>Clean input</i>	12316 MB	29.21
2 Million	14192 MB	19.03
3 Million	16472 MB	22.27
4 Million	18784 MB	24.11
5 Million	23642 MB	24.49
6 Million	36214 MB	28.02
<i>Poison + No Defense</i>	46238 MB	29.08

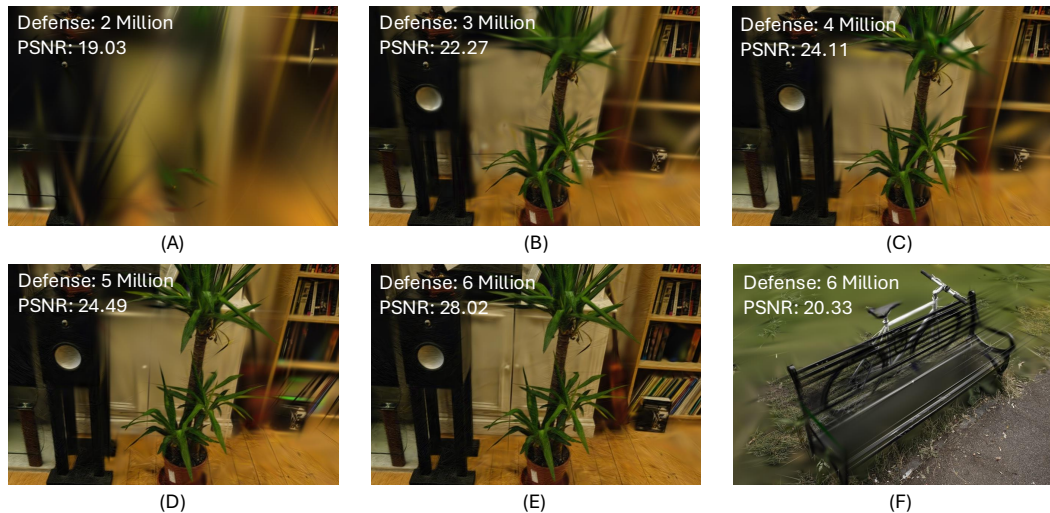


Figure 6: Rendering of reconstructed models under different defense threshold.

As the defense threshold becomes tighter, the maximum GPU memory usage is confined within a safer range. However, this results in a significant drop in the reconstruction’s PSNR, falling to as low as 19.03, which nearly makes it unusable. (c.f. Figure 6 (A)). What’s more, while setting a threshold at 6 million Gaussians appears adequate (achieving PSNR 28.02 dB), this same threshold yields poor rendering results for *bicycle* scene, with only 20.33 dB PSNR (c.f. Figure 6 (F)).

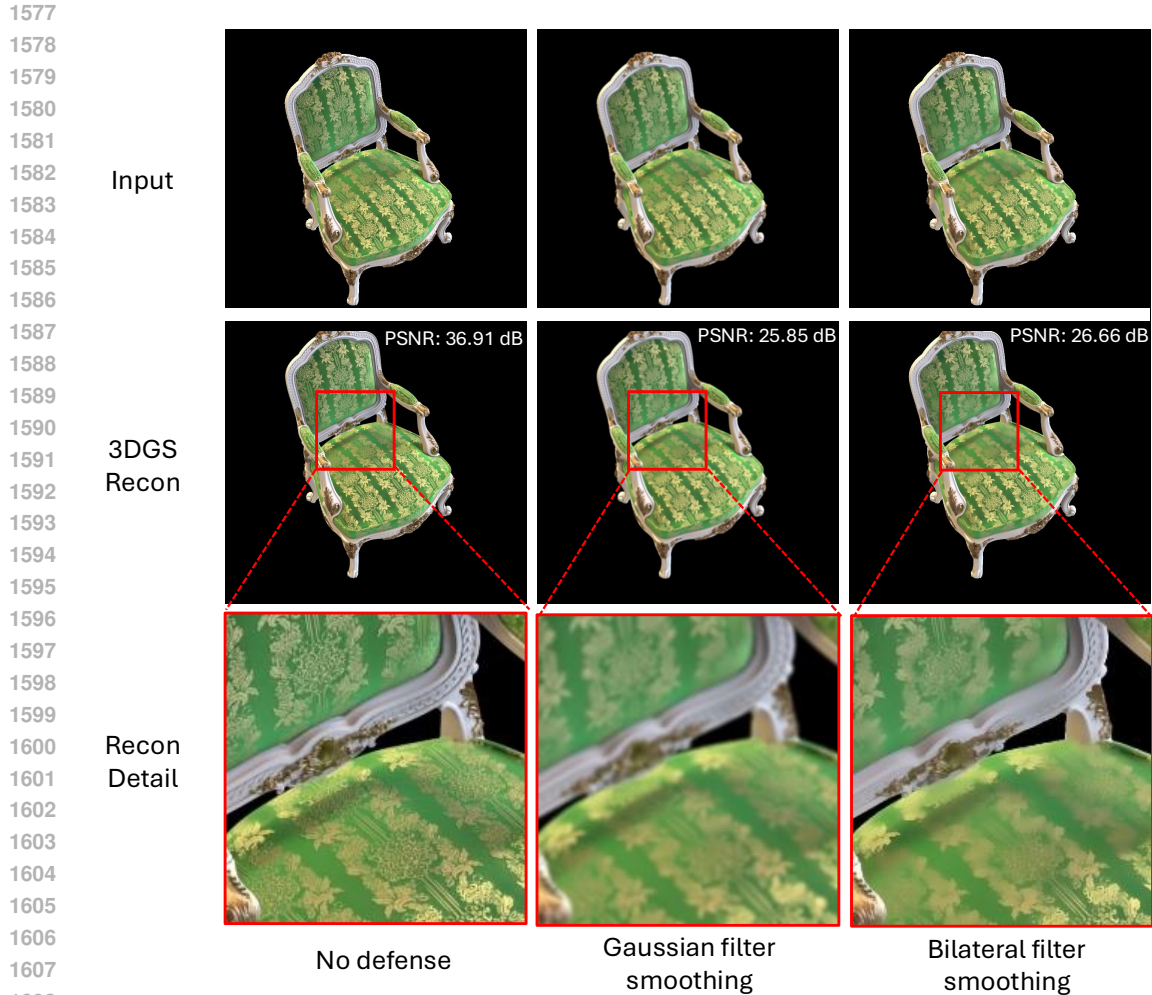
Overall, determining a universal defense threshold that preserves reconstruction quality across various scenes is challenging. Designing a more effective defense against computation cost attack remains an open question, and we hope that future research will continue to explore this area.

J IMAGE SMOOTHING IS NOT AN IDEAL DEFENSE

We will show that image smoothing as a pre-processing to Gaussian Splatting training procedure is not an ideal defense. Without a reliable detection method, defenders may only resort to universally

1566 applying image smoothing to all incoming data. This pre-processing will significantly compromise
 1567 reconstruction quality.

1568 We found that although image smoothing may reduce GPU consumption to some extent, it severely
 1569 undermines efforts to preserve fine image details (Yu et al., 2024; Ye et al., 2024; Yan et al., 2024b).
 1570 As illustrated in Figure 7, applying common smoothing techniques such as Gaussian filtering or
 1571 Bilateral filtering (Tomasi & Manduchi, 1998) leads to a substantial degradation in reconstruction
 1572 quality. For instance, on the *chair* scene of NeRF-Synthetic dataset, reconstruction achieves 36.91 dB
 1573 PSNR without pre-processing; however, with Gaussian or Bilateral filtering, the PSNR drops sharply
 1574 to around 25 dB. This level of degradation is clearly undesirable. Given these challenges, we urge the
 1575 community to develop more sophisticated detection and defense mechanisms against computation cost
 1576 attacks, balancing resource consumption with the preservation of image quality.



1609 Figure 7: Using image smoothing as a pre-processing step can result in unsatisfactory model
 1610 reconstruction quality, particularly regarding fine details in images. This naive defense strategy
 1611 significantly degrades the PSNR by approximately 10 dB, contradicting the primary goal of the
 1612 service provider to maintain high-quality outputs.

1613

1614 K TIME EFFICIENCY OF POISON-SPLAT ATTACK

1615

1616 According to Algorithm 1, we need to solve a bi-level optimization problem, and the time complexity
 1617 is related to T (inner iterations) and \tilde{T} (outer iterations). However in practice, our inner iterations T
 1618 are far fewer than outer iterations \tilde{T} , and the actual time cost of attacker is even less than victim's
 1619 training time, which is an advantage of our attack.

1620 Specifically, the total running time of algorithm 1 is decided by two parts:

- 1621
- 1622 1. Train a proxy model on clean data (Line 2 of Algorithm 1);
 - 1623 2. Solve the bi-level optimization (Line 3 to Line 13 of Algorithm 1)
- 1624

1625 For example, for unconstrained attacks on MIP-NeRF360, we set $T = 6000$ and $\tilde{T} = 25$, and the
 1626 time of attack is totally acceptable, and is even shorter than the victim training, as shown in the
 1627 Table 15 below:

1628 Table 15: Comparison of training times for the attacker and the victim.

1629

1630 Scene	1631 Attacker: Proxy training + Bi-level optimization	1632 Victim: Training time
1633 Bicycle	1634 33.42 + 16.57 min	81.48 min
1635 Bonsai	21.68 + 14.00 min	75.18 min
1636 Counter	26.46 + 15.23 min	62.04 min
1637 Flowers	25.47 + 15.05 min	62.62 min
1638 Garden	33.19 + 15.07 min	83.81 min
1639 Kitchen	26.61 + 14.77 min	73.04 min
1640 Room	25.36 + 16.50 min	76.25 min
1641 Stump	27.06 + 15.63 min	51.51 min

1642 Lastly, the primary motivation of our work is to expose the severity of this security backdoor, and
 1643 attack efficiency is beyond the scope of this paper. We hope to leave the improvement of attack
 1644 efficiency in future studies.

1645
1646
1647
1648
1649
1650
1651
1652
1653
1654
1655
1656
1657
1658
1659
1660
1661
1662
1663
1664
1665
1666
1667
1668
1669
1670
1671
1672
1673